博 士 論 文

A quantitative analysis of bone lamellarity and bone collagen linearity induced by distinct dosing and frequencies of teriparatide administration in ovariectomized rats and monkeys

（卵巣摘出ラットおよびサルにおけるテリパラチドの投与量および投与頻度の違いにより生じる、骨の層板構造および骨コラーゲンの直線性の変化の定量的解析）

令和４年３月申請

北海道大学

大学院歯学院口腔医学専攻

佐　藤　孝　紀

MICROSCOPY

Microscopy, 2021, 498–509
doi:https://doi.org/10.1093/jmicro/dfab020
Advance Access Publication Date: 8 June 2021

Article

A quantitative analysis of bone lamellarity and bone collagen linearity induced by distinct dosing and frequencies of teriparatide administration in ovariectomized rats and monkeys

Takanori Sato[1], Aya Takakura[1,2,*], Ji-Won Lee[1], Kazuaki Tokunaga[3], Haruka Matsumori[3], Ryoko Takao-Kawabata[2,*] and Tadahiro Iimura[1,*]

[1]Department of Pharmacology, Faculty and Graduate School of Dental Medicine, Hokkaido University, N13 W7, Sapporo, Hokkaido 060-8586, Japan; [2]Pharmaceuticals Research Center, Asahi Kasei Pharma Corporation, 632-1 Mifuku, Izunokuni, Shizuoka 410-2321, Japan and [3]Nikon Corporation, 2-15-3 Konan, Minato-ku, Tokyo 108-6290, Japan

*To whom correspondence should be addressed. E-mail: shimomura.ac@om.asahi-kasei.co.jp (A.T.); takao.rb@om.asahi-kasei.co.jp (R.T.); iimura@den.hokudai.ac.jp (T.I.)

Received 16 March 2021; Revised 19 May 2021; Editorial Decision 5 June 2021; Accepted 7 June 2021

Abstract

The lamellar structure of bone, which endows biomechanical rigidity to support the host organism, is observed in mammals, including humans. It is therefore essential to develop a quantitative analysis to evaluate the lamellarity of bone, which would especially be useful for the pharmacological evaluation of anti-osteoporotic drugs. This study applied a current system for the semi-automatic recognition of fluorescence signals to the analysis of un-decalcified bone sections from rat and monkey specimens treated with teriparatide (TPTD). Our analyses on bone formation pattern and collagen topology indicated that TPTD augmented bone lamellarity and bone collagen linearity, which were possibly associated with the recovery of collagen cross-linking, thus endowing bone rigidity.

Key words: bone lamellarity, collagen linearity, multi-photon microscopy, SHG (second harmonic generation), semi-automatic recognition, teriparatide

Introduction

The most characteristic feature of vertebrates is the bone, which is mainly composed of collagen fibers and hydroxyapatite. The evolution of bone has been associated with the development of a hormonal system that regulates mineral metabolism. The parathyroid hormone (PTH) plays key roles in the homeostasis of calcium phosphate through its actions in the bone and kidneys, and indirectly in the intestine [1–3]. Furthermore, the functional evolution of PTH has been thought to be a key event in appearance of terrestrial vertebrates [4–6].

In skeletal ontogeny, primary bone develops in a *de novo* manner, where no bone existed previously, in given parts of fetal mesenchymal tissue, which is structurally termed woven bone. Then, mature bone develops in a manner in which previously formed bone (either woven bone or lamellar bone) is replaced by new lamellar bone [7]. It is understood that woven bone forms when rapid bone formation is required, such as in early skeletal development and bone repair. Thus, woven bone appears to be formed as a 'place-taking' bone for future mature bone formation. Lamellar bone has a highly organized layered structure with well-oriented thick collagen fibers, whereas

woven bone is depolarized hard tissue with randomly oriented and enriched collagen fibrils. Kimmle and Jee estimated that the formation rate of woven bone is six times faster than that of lamellar bone [8]. The lamellar structure of bone is commonly observed in mammals, including humans [9–11], and is proposed to be affected by several factors, including phylogeny, ontogeny, environmental influence and biomechanics [11]. Furthermore, this lamellar structure is incrementally formed. In this formation, new single lamella is deposited on the surface of preformed lamellar bone, which appears to be species-specific and time-dependent [12]. Biochemically, lamellar bone has more enriched non-collagenous proteins, such as bone sialoprotein and osteocalcin, and well-developed calcium phosphate crystals, which are known to be components of mature bone, and it is less susceptible to bone resorption in comparison to those in woven bone [13]. These findings suggest that a slow rate of bone formation is tightly associated with mature bone lamellarity and possibly with maintaining the rigidity of bone such that it is sufficient to sustain the host organism.

Pharmacologically, the exogenous administration of PTH, which promotes bone formation and resorption through its receptor, parathyroid hormone type I receptor depending on whether the administration is intermittent or continuous, has a paradoxical effect in bone [14]. In fact, the intermittent administration of human PTH (1–34) [Teriparatide (TPTD)] and PTH (1–84) are approved as bone anabolic agents for the treatment of osteoporosis [15–18]. Thus, investigation into how different TPTD dosing regimens induce different effects on bone has been a focus of some studies on the pharmacological action of TPTD. To meet clinical requirements, the pharmacological action of TPTD has been evaluated through the parameters of bone formation, bone resorption, bone microarchitecture and bone strength.

Our research group previously reported that the less frequent administration of TPTD (e.g. 3 times/week) more effectively increased the bone mineral density (BMD) and mechanical strength of the lumbar vertebra and femur in an ovariectomized (OVX) rat model in comparison to the frequent administration (e.g. 3 times/day) [19]. This study also revealed that the frequent administration significantly augmented the formation of cortical porosity associated with the increase in bone resorption markers, whereas the less frequent administration was also associated with increased levels of bone formation markers but not with increased levels of bone resorption markers. We also analyzed the effect of the frequency of TPTD administration on rabbit bone with the same total dose but a distinct frequency of administration, such as once-daily or once-weekly. Consistent with the results from rats [18], this work demonstrated that daily but not weekly regimens were associated with the significant development of cortical porosity and marrow fibrosis [20]. Our line of these works therefore demonstrates that the frequency of TPTD administration affects the balance between bone formation and resorption. We also morphologically observed that the low frequency of TPTD administration led to the formation of thicker trabeculae with the maintenance of thick cortices, in comparison to high-frequency administration, suggesting that the frequency of TPTD administration also affects the structural pattern of bone formation, such as bone lamellarity [18,19].

Bone histomorphometry is a unique method that is the gold standard for the evaluation of the rate of bone turnover, which has long been well applied in both basic and clinical bone research [21,22]. However, this morphometric method lacks spatial scores, such as the pattern of bone formation and the lamellarity of bone. Moreover, this method requires a high degree of skill for histological observation and thus shows a degree of subjectivity. This study applied a current semi-automatic recognition system to the non-demineralized histological bone sections with calcian labeling and Villanueva bone staining, which are well-established histomorphometric methods that are used to evaluate the rate of bone turnover. We also subjected these bone sections to collagen imaging by second harmonic generation (SHG) [20,23–27]. To statistically analyze the spatial pattern of bone formation associated with bone collagen, we re-evaluated previously reported rat and cynomolgus monkey bone specimens that were treated with TPTD [19,28,29].

Materials and methods

Animals and experimental design

All experimental protocols were approved by the experimental animal ethics committee of Asahi Kasei Pharma Co., and were conducted in accordance with guidelines concerning the management and handling of experimental animals.

Rats: This study re-examined rat bone specimens that we previously analyzed and reported [19]. Briefly, sexually mature female Sprague-Dawley rats (Charles River, Kanagawa, Japan) of 13 weeks of age were divided into 15 drug regimen groups (Supplementary Fig. 1). Ovariectomy (OVX) or sham surgical operations were conducted under anesthesia, as previously described. At 16 weeks of age, the rats were subcutaneously injected with vehicle saline, or 6 or 30 μg/kg of TPTD acetate (Asahi Kasei Pharma Corporation, Tokyo, Japan), 3 times/week (W3 groups, marked in red); vehicle, 1.2, 6 or 30 μg/kg of TPTD once a day (D1 groups, in orange) or twice a day (D2 groups, in green); and vehicle, 1.2 or 6 μg/kg of TPTD 3 times/day (D3 groups, in blue) for 4 weeks. On the eighth and third days before sacrifice, double-fluorochrome labeling was conducted with two subcutaneous injections of calcein (Dojindo Laboratories, Kumamoto Japan) into each rat at a dose of 10 mg/kg body weight, in order to observe sites of active bone formation.

Monkeys: This study also re-examined the bone specimens of female cynomolgus monkeys (C.V. Universal Fauna, Jakarta Timur, Indonesia), as previously analyzed and reported [28]. Monkeys (age: 12.0 ± 1.5 years, weight: 2.06–3.48 kg) were divided into four groups ($n = 19$–20): (i) the Sham group; (ii) OVX group; (iii) the TPTD-L group, OVX with low-dose TPTD (1.2 μg/kg, once a week); and (iv) the TPTD-H group, OVX with high-dose TPTD (6.0 μg/kg, once a week) (Supplementary Fig. 2). OVX and sham operations were carried out 1 week before TPTD treatment. TPTD or saline (as a vehicle) was subcutaneously injected once a week, for 18 months (Supplementary Fig. 2a). To determine bone formation rates and sites of active mineralization, double-fluorochrome labeling with intravenous calcein injection (4 mg/kg; Dojindo Laboratories, Kumamoto, Japan) at Days 7 and 21 before sacrifice was conducted for all monkeys.

Bone histomorphometry and selection of specimens for the semi-automatic imaging analysis

Bone histomorphometry was performed on the sagittal sections of second lumbar vertebra from all monkey specimens to evaluate bone mass, structure and bone metabolism (resorption and formation) in cancellous bone using an image analysis system (Histometry RT Camera, System Supply, Nagano, Japan; OsteoMeasure, Decatur, GA, USA). The nomenclature, symbols and units used in this study are those recommended by the Nomenclature Committee of the

American Society for Bone and Mineral Research [21,22]. The following three classified parameters were measured: static parameters (trabecular bone volume [bone volume/tissue volume {BV/TV}], trabecular bone surface [BS]/BV, trabecular thickness, trabecular number and trabecular separation), a bone resorption parameter (eroded surface/BS), and bone formation parameters (mineralizing surface/BS, single- and double-labeled surface BS, and bone formation rate/BV).

As a further semi-automatic imaging analysis, we selected three specimens from each of four regimen setting groups (19–20 specimens) that showed histomorphometric scores nearest to the mean value (Supplementary Figs. 2b and c). These selected samples were subjected to SHG imaging.

Differential interference contrast and fluorescence imaging

Differential interference contrast (DIC) imaging and fluorescence imaging were obtained using a microscopy system, ECLIPSE Ni (Nikon, Tokyo, Japan) equipped with a DIC microscope and objectives (Nikon) Plan Apo λ ×10 (numerical aperture [NA] = 0.45), Plan Apo λ ×20 (NA = 0.75) and Plan Apo λ ×40 (NA = 0.95). The fluorescence signals were obtained using filter sets, fluorescein isothiocyanate (FITC) (excitation: 460–500 nm, dichroic mirror (DM): 505 nm, emission: 510–560 nm; Nikon) for calcein and TxRed (excitation: 540–580 nm, DM: 595 nm, emission: 600–660 nm; Nikon) for autofluorescence derived from soft tissue. Tiling fluorescence imaging to acquire the entire, high-contrast view of the tissue sections was carried out using the Plan Apo λ ×10 objective (NA = 0.45). The frame size of a single scan was 1280 × 1024 pixels, with an 8-bit color depth. The fluorescence and DIC images were sequentially acquired, with a pixel size of 0.64 μm. In the case of SHG imaging, image processing was performed using the NIS-Elements AR imaging software program (Nikon, Tokyo, Japan).

Second harmonic generation imaging

SHG imaging of monkey seventh lumbar vertebra was carried out using an upright multi-photon excited microscopy system (A1RMP, Nikon, Tokyo, Japan) at the Imaging Core facility of the Institute of Medical Science, the University of Tokyo, to observe bone collagen that emits SHG signals via nonlinear excitation phenomena. The microscope was equipped with a water-immersion objective lens (Apo LWD 40×, NA: 1.15WIλS, Nikon) and a Chameleon laser oscillator (COHERENT, Inc. CA). The excitation wavelength was 880 nm. The detection wavelength for the acquisition of collagen-derived SHG signals was 446 nm. Three-dimensional (3D) images were acquired by taking 20 optical slices with a step size of 4.0–4.5 μm and a pixel size of 2.49 μm. Image processing, including 3D projection and 3D rendering, were performed using the NIS-Elements AR imaging software program (Nikon).

Semi-quantitative fluorescence morphometry and automatic morphometric recognition analyses using artificial intelligence and deep learning

Quantitative topological analyses of fluorescence signals in undecalcified bone sections in the current study were established with the application of commercially available imaging analysis tools (NIS-Elements AR and NIS.ai, Nikon, Tokyo, Japan). The following parameters of recognized objects were semi-automatically measured: object number, length, perimeter, outer perimeter, width, object area, object fill-area, orientation and smoothness (hull convex perimeter/perimeter). Examples of the measurement parameters for the analyses of trabecular bone, calcein labeling and collagen fibers are schematically illustrated in Supplementary Fig. 3a, b and c, respectively. Binarization of objects was interactively conducted using the fluorescence intensity threshold, object size and manual histomorphological definition. The recognition of objects was set as follows: trabecular bone (threshold 200, size > 50.0 μm), fibrous collagen (threshold 800, size > 40.0 μm), soft tissue (threshold 10, size > 50.0 μm) and calcein labeling (threshold 50, size > 5.0 μm). The automatic morphometric recognition of osteocytes was carried out by artificial intelligence (AI) and deep learning methods (NIS.ai) with the detection of autofluorescence signals derived from osteocytic lacunae after conducting morphological recognition learning more than 1000 times.

In the measurement of monkey samples, the region of interest was a rectangular form (vertical 2.0 mm; horizontal 2.5 mm). The region was ≥1.0 mm from the cortical bone and growth plate. In the measurement of rat samples, a square form (vertical 1.0 mm; horizontal 1.0 mm) was selected. The region was ≥0.2 mm from the cortical bone.

Statistical analysis

All data are presented as mean ± standard error (SE). The effects of TPTD on bone specimens were evaluated using an analysis of variance. In the rat study, Dunnett's test was applied to compare the treatment and vehicle control group with each frequency of administration. In the monkey study, Dunnett's test was applied to compare with OVX group. In both studies, *P*-values of <0.05 were considered to indicate statistical significance.

Results

By taking full advantage of current histological fluorescence morphometry with a commercially available semi-automatic recognition system, we first analyzed the BV/TV in rat vertebrae in 15 TPTD regimen settings, as we previously reported [19] (Fig. 1, and Supplementary Fig. 1). In this analysis, the BV/TV was measured by measuring the area of autofluorescence derived from soft tissue in histological sections subjected to Villanueva bone staining (Fig. 1a, and Supplementary Fig. 4). The bone area was measured by subtraction of this soft tissue area from the measured total tissue area. This analysis demonstrated that the administration of TPTD augmented the BV/TV in a clear dose-dependent manner at all four frequencies of administration (3 times/week and 1, 2 and 3 times/day) (Fig. 1b and c, and Supplementary Fig. 5). This analysis showed exactly the same pattern as our previous analysis of BMD measured by dual-energy X-ray absorptiometry [19]; thus, this analytical method was well validated.

We next applied the semi-automatic recognition system to fluorescence morphometry of bone areas labeled by calcein. We set parameters, such as the area, length, outer perimeter and number of calcein-labeled signals using the measurement function provided by the system, and performed comparative scoring (Fig. 2, and Supplementary Fig. 3a and b). Interestingly, in the 3 times/week and 1 time/day groups, the scores of area, length and outer perimeter were increased in a dose-dependent manner, while the number was decreased in a dose-dependent manner (Fig. 2b). These tendencies were less obvious in the 2 times/day and 3 times/day groups. Notably, in the 2 times/day group, the highest dose (30 μg/kg) of

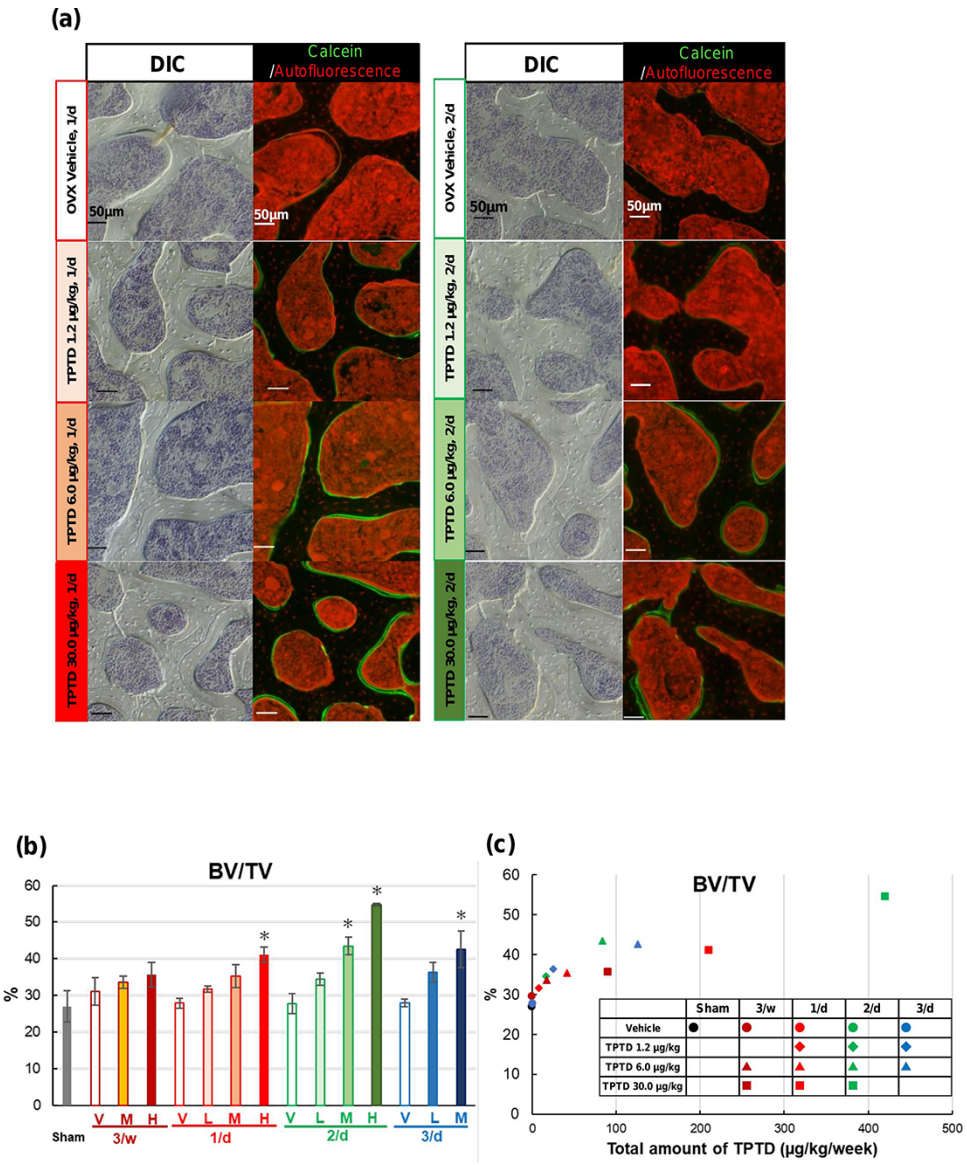

Fig. 1. The anabolic effect of TPTD on BV of rat vertebral trabeculae, as quantified by a semi-automatic recognition system. (a) Representative DIC (left panels) and corresponding fluorescence images of rat vertebral trabeculae treated with the indicated regimens of TPTD. In the right panels, fluorescence signals derived from calcein and autofluorescence of soft tissues are shown in green and red, respectively. Scale bars indicate 200 μm. (b, c) Quantitative and statistical analyses of BV/TV by a semi-automatic recognition system are shown. Data are shown as mean. *Indicates $P < 0.05$ vs. vehicle for each frequency of administration (Dunnett's test).

TPTD did not augment the scores of the labeled area, length and outer perimeter in comparison to a dose of 6 μg/kg. The calcein-labeled length/bone perimeter showed a similar pattern to the length, while the width of calcein labeling did not differ to a statistically significant extent, except in the 2 times/day group, which showed a dose-dependent increase (Supplementary Fig. 6). In this analysis, a dose-dependent increase in bone formation length by TPTD was only observed at lower administration frequencies of 3 times/week and 1 and 3 (but not 2) times/day (Fig. 2, and Supplementary Figs. 6 and 7) [19,28,29].

To confirm that these parameters in calcein-labeled tissues were increased by the administration of TPTD in another experimental animal treated with TPTD for a longer period (where the pharmacological effect of TPTD appears to be saturated), we re-examined the same experimental set of monkey specimens with four distinct regimen groups (Sham, OVX, TPTD-L [1.2 μg/kg] and TPTD-H [6 μg/kg]) with once-weekly administration for 18 months, as previously reported (Fig. 3, and Supplementary Fig. 2). To subject these monkey specimens to further semi-automatic analyses, we needed to select small numbers of specimens from the four experimental groups for acquisition of whole 3D SHG images of entire vertebral body sections (size, ~1 × 2 cm; depth, 300–400 μm). For this purpose, we initially conducted conventional bone histomorphometry in all specimens. There were no significant differences in parameters such as BV/TV, BS/BV, trabecular thickness, trabecular number, trabecular separation, single-labeled surface/BS,

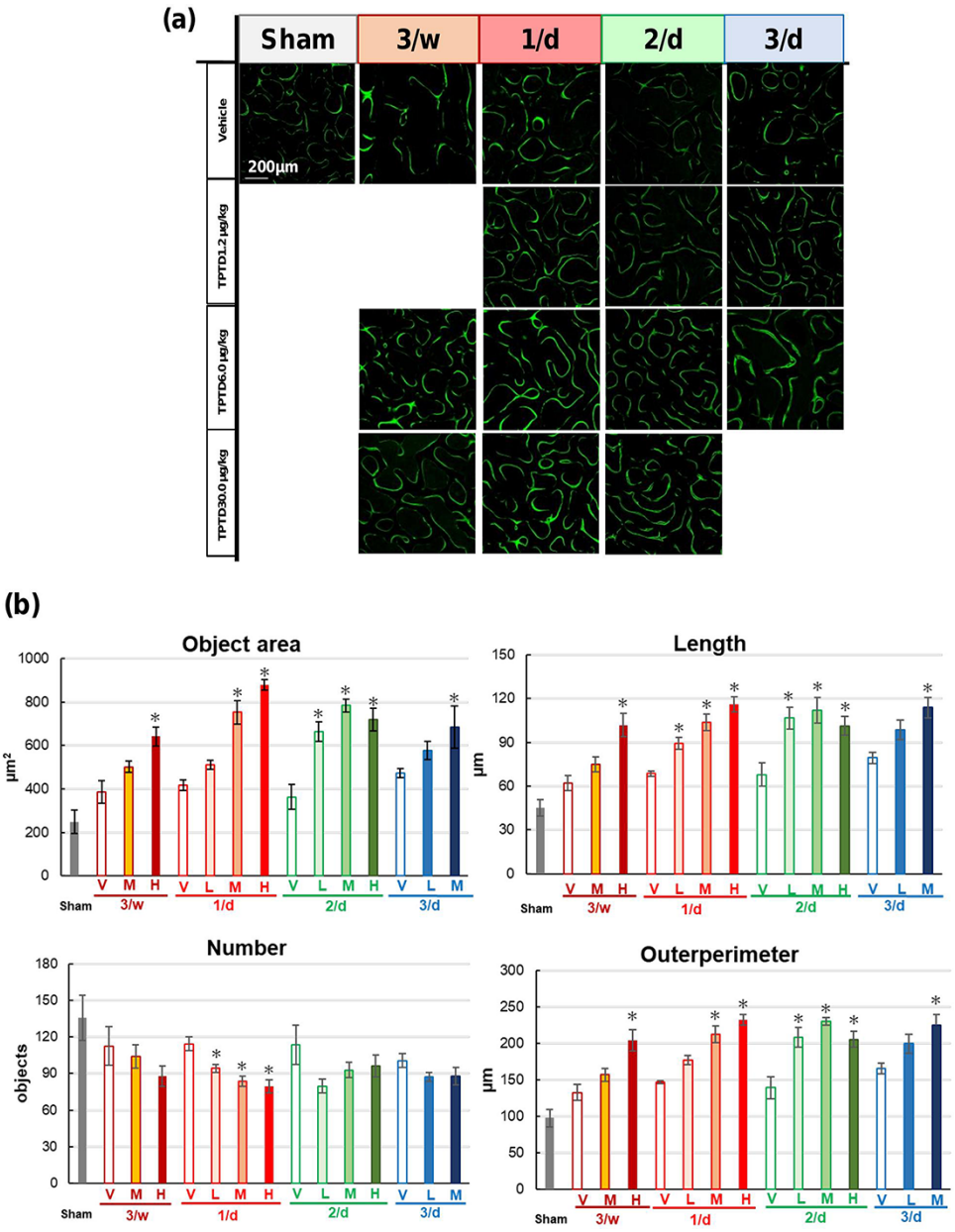

Fig. 2. The quantitative topological analysis of bone formation patterns by morphometry of calcein signals in rat vertebral trabeculae. (a) Representative calcein-derived fluorescence images of rat vertebral trabeculae treated with TPTD at the indicated regimens. These are magnified views of the region of interest framed by white dotted squares in Supplementary Figure 4. Scale bars indicate 200 μm. (b) The topological parameters of calcein signals, such as object area, length, number and outer perimeter were measured and statistically compared. Data are shown as mean. * Indicates $P < 0.05$ vs. vehicle for each frequency of administration (Dunnett's test).

double-labeled surface/BS, mineralizing surface/BS, bone formation rate/bone and surface (bone formation rate/BV) (Supplementary Fig. 8, Supplementary Table 1a), which was consistent with a previous report [29]. Based on this morphometric analysis, we selected three representative specimens from each of the Sham, OVX, TPTD-L and TPTD-H experimental groups. A bone morphometric analysis of these selected specimens did not show any significant differences (Supplementary Figs. 2 and 9, Supplementary Table 1b), thus indicating that our selection of specimens in this step was not biased. These representative specimens from each experimental group were subjected to further analyses.

In the trabecular bonein the vertebrae of this model animal, the area and length of calcein-derived signals were decreased, albeit not significantly, in the OVX group in comparison to the Sham group (Fig. 3). These parameters in the TPTD-H group were recovered to the level in the Sham group, whereas the average width was the same (Fig. 3).

The combinatorial observation of bone tissues with a DIC microscope and these quantitative analyses of the calcein-labeled tissue area made us notice that the spatial distribution, such as the linearity of the labeled tissue, was associated with lamellar structure formation of trabecular bone in the rat and monkey models

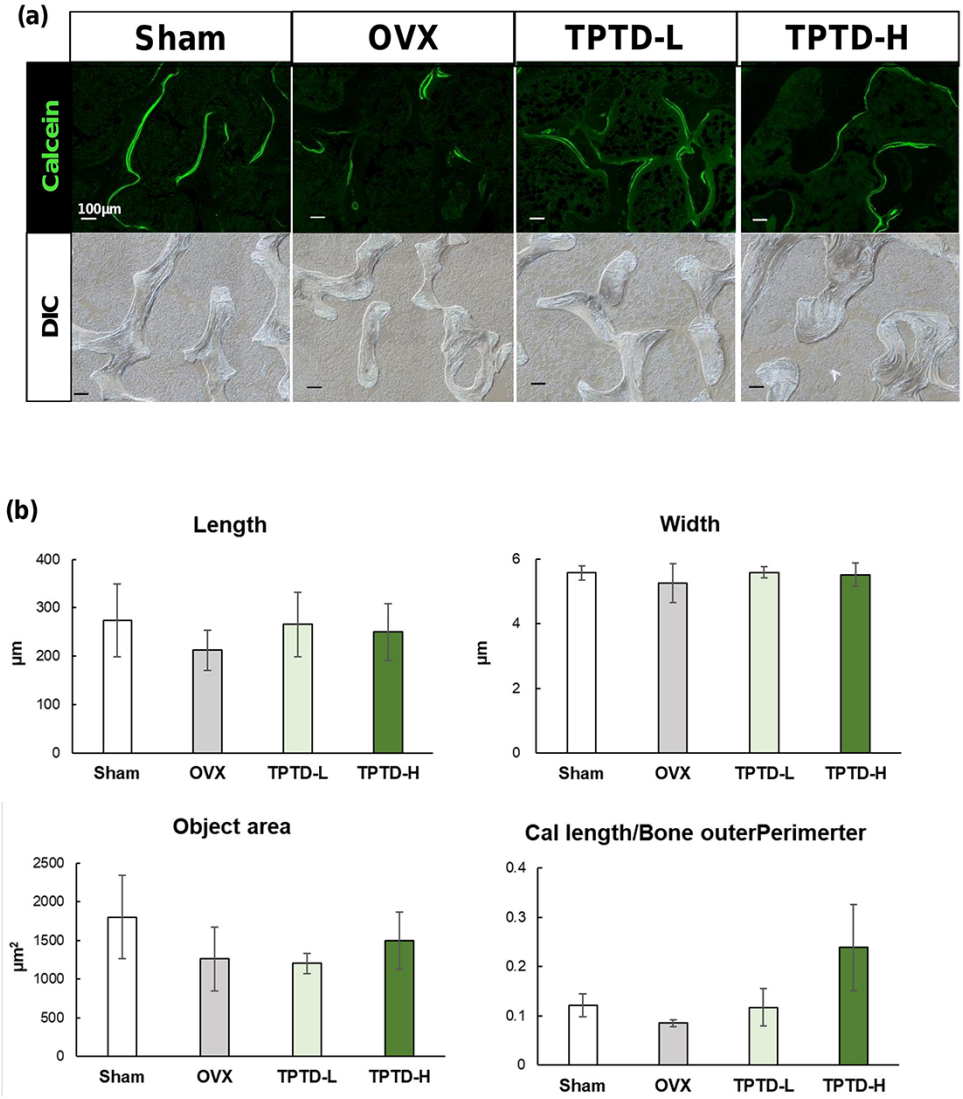

Fig. 3. The quantitative topological analysis of bone formation patterns by morphometry of calcein signals in monkey vertebral trabeculae. (a) Representative calcein-derived fluorescence images of monkey vertebral trabeculae treated with the indicated TPTD regimens. Scale bars indicate 100 μm. (b) Topological parameters of calcein signals, such as object area, length, width and calcein length/bone outer perimeter, were measured and statistically compared. Data are shown as mean ± SE. *P*-values vs. OVX group did not show statistical significance (Dunnett's test) ($P > 0.05$).

(Figs. 1a and 3a). This finding prompted us to take advantage of the application of nonlinear optics, which enabled us to visualize fibers or bundles of collagen in organic tissues by SHG. We conducted large tiling and 3D imaging of whole sagittal sections of monkey vertebral bodies (Fig. 4a and b). Intense SHG-derived fluorescence signal was observed in whole bone tissue, including the inner trabecular bone and outer cortical bone, but not in cartilage or soft tissues, such as bone marrow. Intense fibrous signals that extended multidirectionally in bone tissue were clearly recognizable, while relatively weak and broad signal covers whole bone tissue. Therefore, for morphometrical analyses based on SHG signal, we set up two types of threshold: an intense threshold to detect fibrous collagen and a mild threshold to detect bone tissue through binarization of object size and signal intensity (Fig. 5, and see Materials and Methods). We measured the size, area, length and width of the fibrous SHG signals (Fig. 6) and compared these parameters in the four TPTD administration groups. The average number of fibrous SHG signals/tissue area (N.SHG) in the OVX group was higher than that in the Sham group, but not to a statistically significant extent (Fig. 6). The administration of TPTD tended to reduce N.SHG in a dose-dependent manner. In contrast, the average area and length of the fibrous SHG signal (Area SHG and Length SHG, respectively) were decreased in the OVX group, while these showed a dose-dependent recovery with the administration of higher dose of TPTD: TPTD-H (Fig. 6). In comparison to these parameters, the width of the fibrous SHG signal did not show much difference in these four groups (Fig. 6). The average number of fibrous SHG signals/bone area (N.SHG/bone) and the average area of fibrous SHG signal/bone area (Area SHG/bone) showed tendencies that were consistent with the corresponding parameters of the N.SHG and Area SHG (Fig. 6). The analyses of these parameters demonstrated that the administration to OVX monkeys augmented the length but not the number

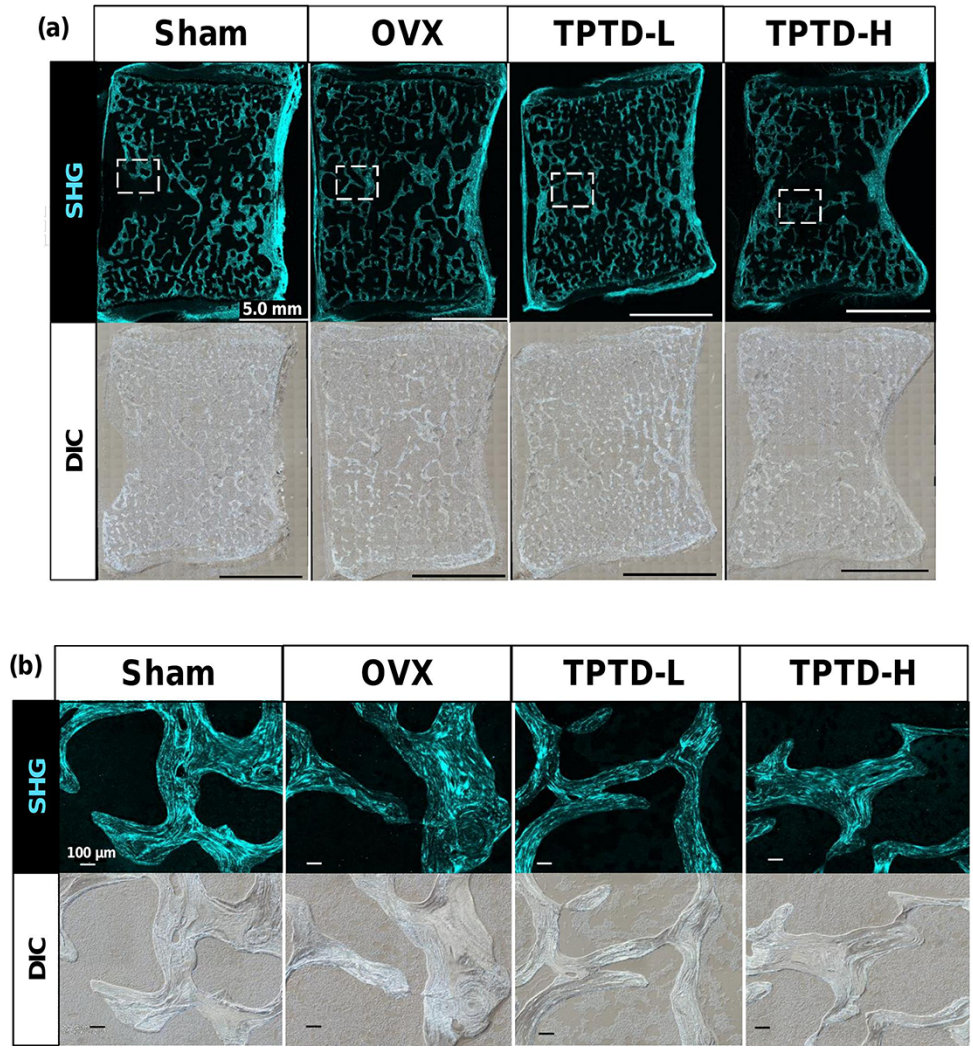

Fig. 4. SHG and DIC tiling images of monkey vertebral trabeculae. (a) Representative SHG (upper panels) and corresponding DIC tilling images were acquired from the Sham group, OVX group, PTH-L (low-dose TPTD) group and PTH-H (high-dose TPTD) group. Scale bars indicate 5.0 mm. (b, c) The mid-dorsal portions framed by dotted boxes in the corresponding images shown in (a) are magnified. Corresponding DIC images are also shown for morphological comparison. Scale bars indicate 100 μm.

of bone collagen fibers. Consistently, the smoothness of the fibrous SHG signal (Smo.SHG) tended to be increased by the administration of TPTD in comparison to that in OVX (Fig. 6). The orientation of SHG signals in the TPTD-H group showed an increase in the horizontal direction (Supplementary Fig. 10). Therefore, it was suggested that the administration of TPTD induced the linear and isotropic distribution of collagen fibers, whereas fractioned and anisotropic distribution of collagen was observed in OVX.

We further applied an AI-based recognition system for counting the number of osteocytes that were differentiated from osteoblasts—a number that reflects the pattern and rate of bone formation (Fig. 7). Specimens in the TPTD-H group tended to show greater numbers of osteocytes/bone area, suggesting correlations with length SHG and width SHG.

Discussion

This study applied a current semi-automatic recognition system to the non-demineralized histological bone sections with calcein labeling and Villanueva bone staining. We have noticed that autofluorescence at a wavelength of ∼560 nm from these bone sections clearly demarcate soft tissues and cells, such as bone marrow, muscle, tendon and osteocytes embedded in bone. We quantified the morphometric parameters of this autofluorescence and calcein-derived fluorescence signal that demonstrated pattern of bone formation.

To confirm the reliability of our approach, we measured the BV/TV in rat vertebrae in 15 TPTD administration groups [19]. The data we obtained were consistent with our previous analysis of BMD measured by dual-energy X-ray absorptiometry [19]. Conventional bone morphometry is performed manually and requires specialized knowledge and skills, and—to some extent—cannot exclude potential subjectivity, especially in the quantification of histological specimens. However, our semi-automatic recognition system enabled the comprehensive measurement and analysis of biometric information more easily and quickly than conventional systems, thus excluding subjectivity. Some clinical attempts to grasp osteoporotic fractures by applying a semi-automatic morphometric method using digital imaging have been reported [30,31]; however, a completely

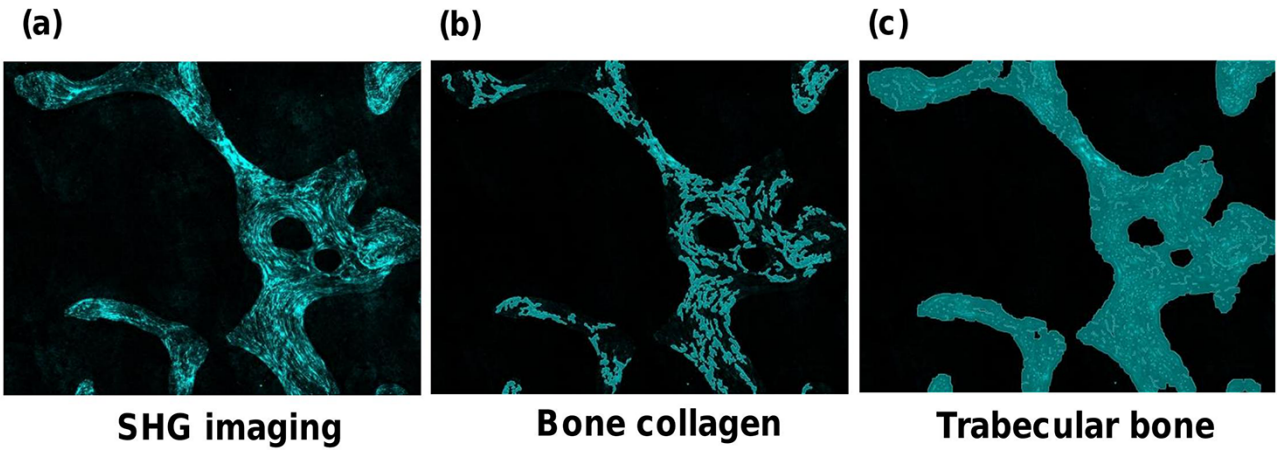

Fig. 5. Binarization of SHG images for the analysis of monkey bone collagen and trabeculae. (a) Raw data of SHG imaging of monkey vertebral trabeculae. (b, c) Corresponding binary images to those of bone collagen fibers and trabecular bone (shown in [a]). The threshold conditions for visualization of bone collagen and trabecular bone are indicated. In the analyses of bone collagen and trabeculae, the object sizes are >40 μm and >50 μm, while the luminance intensities of the objects are >800 and >200, respectively.

automatic level has not yet been achieved. Therefore, the development of an AI-based recognition system in the near future would be beneficial to biometric informatics.

We next applied this semi-automatic recognition system to the analysis of fluorescence signals from calcein labeling. In conventional histomorphometry, calcein-based parameters reflect the bone formation surface and rate; however, they lack information on spatial patterns of bone formation. Our parameter analysis, which measured the number, area, length, outer perimeters and smoothness of the calcein-labeled area, provided a method for the quantification of spatial patterns of bone formation. This analysis demonstrated the linearity of calcein signaling—possibly due to synchronicity of bone formation—was augmented by the administration of TPTD in a dose-dependent manner. This analysis further indicated that the excess amount and frequency of administration rather negatively affected the synchronicity of bone formation, which would not have been noticed by conventional histomorphometry methods. Interestingly, our calcein length analysis did not demonstrate a dose-dependent increase in bone formation surface especially in the group of 2 times/day (shown in Fig. 2b), while BV/TV obviously showed a dose-dependent increase in BV (shown in Fig. 1b). These findings appeared to be inconsistent, however, can be interpreted as a way that concave trabecular surfaces were getting filled with new bone formed by higher TPTD administration, thus these BSs became flattened, which could cause shorter calcein labeling. In fact, this phenomenon was often observed in our series of previous pharmacological works of TPTD, but failed to be demonstrated in a quantitative way. Therefore, this analysis is available to quantitatively demonstrate the spatial patterns of bone formation.

Bright-field DIC images showed that the increased linearity of calcein labeling observed after TPTD treatment was highly associated with the lamellar structure of bone. It has been reported that the visual appearance of the lamellar structure of bone is formed by the repeated appearance of collagen-rich (dense or thin lamellae) surface and collagen-poor (loose or thick lamellae) surface [32–34], which prompted us to visually quantify the topological characteristics of the bone collagen. We took advantage of advanced nonlinear optics imaging (SHG) using a multi-photon microscopy system, which enabled the visualization of bone collagen fibers so that we could apply our semi-automatic recognition system to measure the spatial pattern of the bone collagen fibers of bone specimens obtained from cynomolgus monkeys of the TPTD regimen set reported by Saito *et al.* [28].

After a relatively long period of TPTD treatment (18 months), none of the histomorphometric parameters in monkeys showed significant differences, indicating that the increased bone turnover induced by once-weekly TPTD treatment had already plateaued during the long treatment period in these monkey specimens, which was consistent with a previously reported observation in relation to the same monkey specimens [29]. However, a biochemical analysis of collagen cross-link properties of the same monkey specimens demonstrated that low-dose and high-dose TPTD treatments increased the content of enzymatic immature and mature cross-links and decreased advanced glycation end product cross-links, such as pentosidine, in comparison to the OVX group [28]. In our imaging analyses of the same monkey specimens in this study, the average length/bone perimeter (bone formation surface/bone perimeter) in the monkey OVX group tended to decrease in comparison to that in Sham group, while these parameters appeared to recover—in a dose-dependent manner—by the administration of TPTD. Similarly, the average length and area of the collagen fiber–derived SHG signal (Length SHG and Area SHG, respectively) in the OVX group also tended to decrease in comparison to the Sham group, while these parameters recovered—in a dose-dependent manner—with the administration of TPTD. The numbers of collagen fiber–derived SHG signals in the four experimental groups showed an inversed pattern with respect to length and area. Furthermore, the smoothness of the fibrous SHG signal (Smo.SHG) tended to be increased by the administration of TPTD. Although changes in these parameters were not statistically significant possibly due to lack of enough sample size ($N = 3$/group), they were consistent with the results of a calcein-labeling analysis in rats as mentioned earlier. These analyses, therefore, suggested that the spatial arrangement of collagen fibers in the OVX group was fractioned and anisotropic, whereas TPTD treatment enhanced the linear and

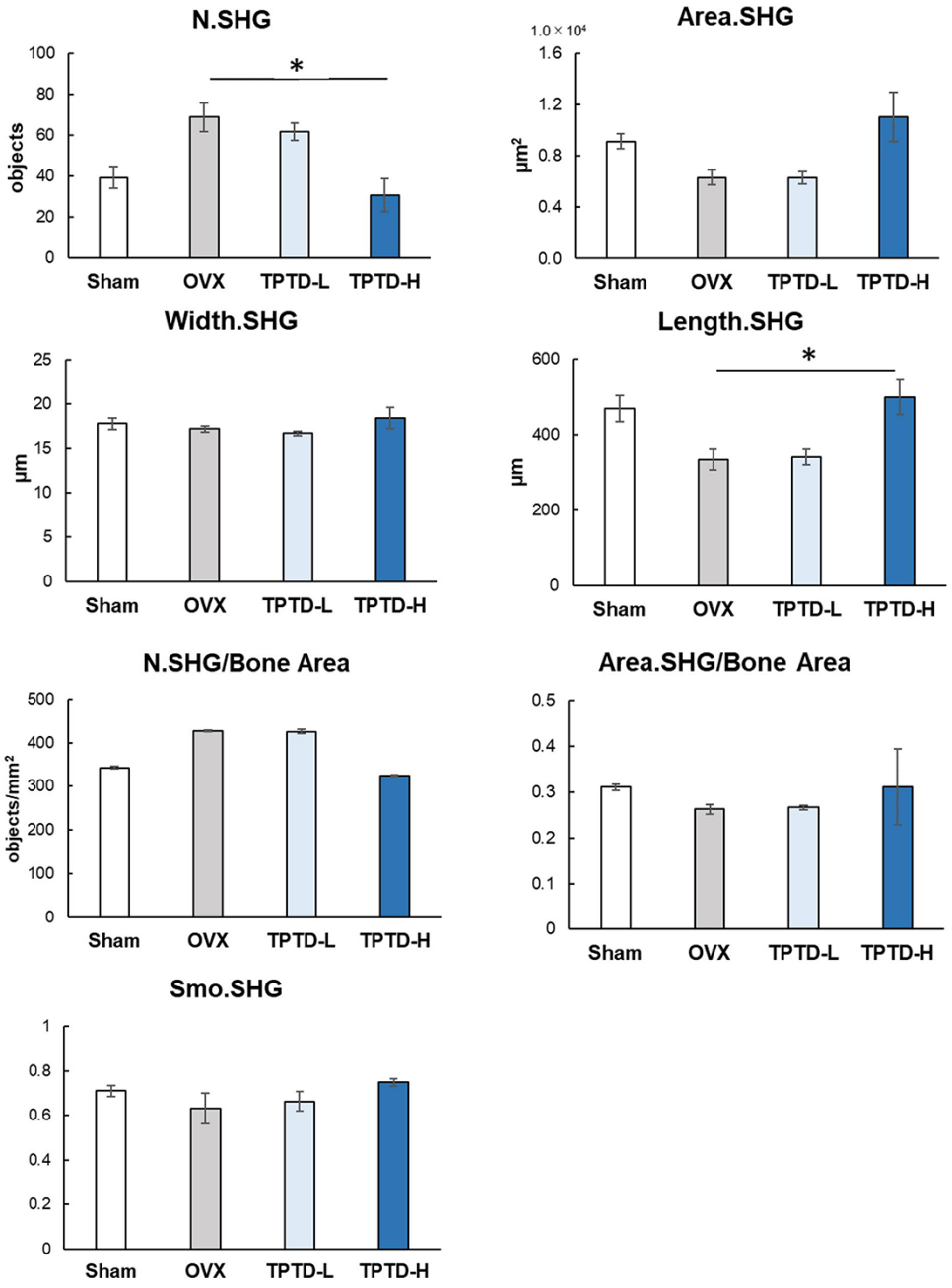

Fig. 6. Quantitative analyses of bone collagen spatial patterns. The topological parameters of SHG signals, such as the number, object area, length, width, number/bone area and smoothness were measured and statistically compared. Data are shown as mean ± SE. * Indicates $P < 0.05$ vs. OVX group (Dunnett's test).

isotropic arrangement of collagen fibers and the lamellarity of the trabecular bone microstructure, even after a long treatment period in which the pharmaceutical effects on bone turnover by TPTD was less evident.

In terms of the clinical aspect and pharmacology of TPTD, it is relevant to consider how the enhanced linear collagen arrangement and bone lamellarity contribute to improving the mechanical properties of bone to reduce the fracture risk. Recent studies reported that the connectivity of the collagen network is an essential factor for evaluating the toughness of bone [28,35,36]. The flexibility of physiological enzymatic cross-links of collagen fibers enables the bone matrix to be sufficiently deformed to facilitate energy dissipation [36], whereas the cross-linking by advanced glycation end products that is associated with aging and metabolic disease, such as diabetes, over-stabilize bone collagen, leading to the presentation of brittle bone and a reduction of bone toughness [28,35,36]. Accordingly, smooth linear sliding between collagen molecules is a critical factor for achieving energy dissipation, which can be facilitated by physiological enzymatic cross-links and the linear arrangement of collagen fibers [36]. Therefore, our analyses demonstrated that

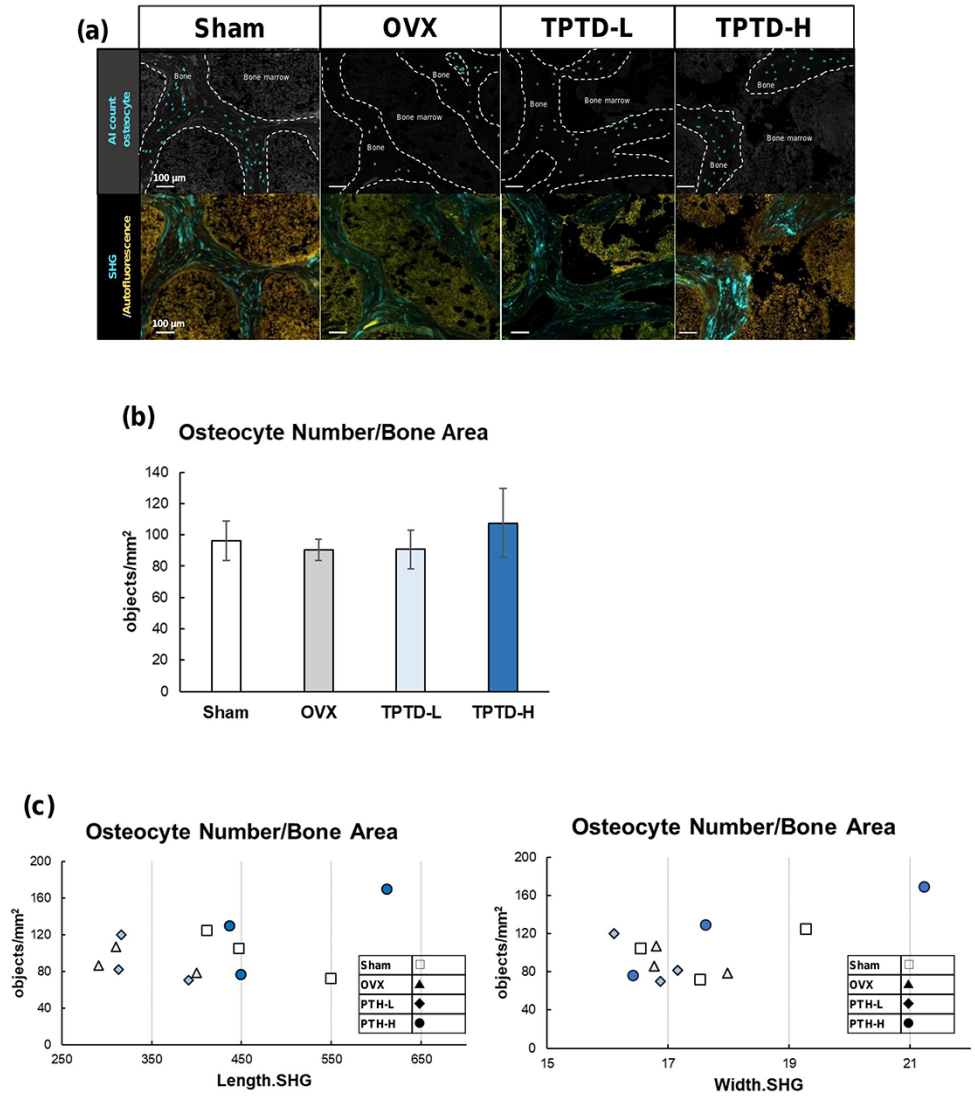

Fig. 7. Automatic morphometric recognition analyses of osteocytes using AI and deep learning. (a) Representative views of AI-based morphometric recognition of osteocytes (upper panels) at indicated TPTD administration regimens and corresponding SHG and autofluorescence images (lower panels). (b) The average osteocyte number/bone area was compared ($N = 3$). (c) The osteocyte number/bone area was plotted for the four administration regimens. Open square, closed triangle, closed diamond and closed circle indicate specimens from the Sham group, OVX group, TPTD-L group and TPTD-H group, respectively. $R = 0.36$ and 0.45.

TPTD treatment enhanced the mechanical properties of bone, not only through the recovery of healthy cross-links but also through the augmentation of the linearity of collagen fibers and the lamellarity of the bone microarchitecture.

Our study demonstrated the changes in properties of collagen fibers and bone formation patterns that occur with the administration of TPTD, focusing on bone lamellarity. In particular, it is significant that the topological character of bone collagen was visualized and quantified by SHG imaging and a semi-automatic morphology recognition system. Our approach here fills the gap between collagen motion—at the sub-nano scale to macro scale—in the bone hierarchical structure [37–39]. Collagen is the main structural protein in bone and contributes to bone toughness by dissipating energy via its deformation [37,40]. At the sub-nano scale to sub-micro scale, the deformation of collagen fibers plays an important role in the energy dissipation, as discussed above [35,37,39]. However, at the microscale, the discussion on bone structures associated with bone toughness moves to structural features of bone, such as trabecularity and density [37,39]. Accordingly, it is relevant to analyze the spatiotemporal arrangement of collagen fibers [34]. This study enabled us to statistically compare the topological characteristics of collagen fibers of bone at the micro scale. In conclusion, an increase in the linearity of collagen fibers, as well as an increase in bone formation surface and area, contributes to the endowment of bone with more toughness by dissipating energy. Thus, collagen linearity is a relevant parameter for estimating the bone toughness pharmacologically imposed by the administration of TPTD.

Concluding remarks

Our study demonstrated the changes in bone formation patterns and collagen fiber properties that occurred with the administration

of TPTD. In particular, it is significant that the topological character of bone collagen in conventionally prepared bone sections was visualized and quantified by the application of SHG imaging and a semi-automatic morphology recognition system. Therefore, our approach in this study will highly contribute to pharmaceutical evaluation of anti-osteoporotic drugs, bone biomedicine and the evolutional biology of bone.

Funding

This work was partly supported by Grant-in-Aids for Scientific Research from the Japan Society for the Promotion of Science (JSPS KAKENHI) grant numbers 18H02983 and 18K19649 to T.I. J.W.L. was supported by Grant-in-Aids for Scientific Research from the Japan Society for the Promotion of Science (19K10044) and a grant from Takeda Science Foundation.

Acknowledgements

We express sincere thanks to Masako Ino at Nikon Solutions for her expertise in microscopy imaging and image processing.

Conflict of interest statement

A.T. and R.T.K. are employees of Asahi Kasei Pharma Corporation. K.T. and H.M. are employees of Nikon Corporation. The remaining authors declare no conflicts of interest in association with the present study.

Supplementary data

Supplementary data are available at *Microscopy* online.

References

1. Potts J T (2005) Parathyroid hormone: past and present. *J. Endocrinol.* 187: 311–325.
2. McCauley L K and Martin T J (2012) Twenty-five years of PTHrP progress: from cancer hormone to multifunctional cytokine. *J. Bone Miner. Res.* 27: 1231–1239.
3. Ruben J A and Bennett A A (1987) The evolution of bone. *Evolution* 41: 1187–1197.
4. Suarez-Bregua P, Chien C J, Megias M, Du S, and Rotllant J (2017) Promoter architecture and transcriptional regulation of musculoskeletal embryonic nuclear protein 1b (mustn1b) gene in zebrafish. *Dev. Dyn.* 246: 992–1000.
5. Suarez-Bregua P, Saxena A, Bronner M E, and Rotllant J (2017) Targeted Pth4-expressing cell ablation impairs skeletal mineralization in zebrafish. *PLoS One* 12: e0186444.
6. Suarez-Bregua P, Torres-Nunez E, Saxena A, Guerreiro P, Braasch I, Prober D A, Moran P, Cerda-Reverter J M, Du S J, Adrio F, Power D M, Canario A V, Postlethwait J H, Bronner M E, Canestro C, and Rotllant J (2017) Pth4, an ancient parathyroid hormone lost in eutherian mammals, reveals a new brain-to-bone signaling pathway. *FASEB J.* 31: 569–583.
7. Bonewald SLD L F and Gorski J P (2009) Bone mineralization. In: Pourquie O ed., *The Skeletal System*, pp 277–295 (Cold Spring Harbor Laboratory Press, New York).
8. Kimmel D B and Jee W S (1980) A quantitative histologic analysis of the growing long bone metaphysis. *Calcif. Tissue Int.* 32: 113–122.
9. Weiner S, Traub W, and Wagner H D (1999) Lamellar bone: structure-function relations. *J. Struct. Biol.* 126: 241–255.
10. Razi H, Predan J, Fischer F D, Kolednik O, and Fratzl P (2020) Damage tolerance of lamellar bone. *Bone* 130: 115102.
11. Kolb C, Scheyer T M, Veitschegger K, Forasiepi A M, Amson E, Van der Geer A A, Van den Hoek Ostende L W, Hayashi S, and Sánchez-Villagra M R (2015) Mammalian bone palaeohistology: a survey and new data with emphasis on island forms. *PeerJ* 3: e1358.
12. Bromage T G, Lacruz R S, Hogg R, Goldman H M, McFarlin S C, Warshaw J, Dirks W, Perez-Ochoa A, Smolyar I, Enlow D H, and Boyde A (2009) Lamellar bone is an incremental tissue reconciling enamel rhythms, body size, and organismal life history. *Calcif. Tissue Int.* 84: 388–404.
13. Gorski J P (1998) Is all bone the same? Distinctive distributions and properties of non-collagenous matrix proteins in lamellar vs. woven bone imply the existence of different underlying osteogenic mechanisms. *Crit. Rev. Oral Biol. Med.* 9: 201–223.
14. Silva B C, Costa A G, Cusano N E, Kousteni S, and Bilezikian J P (2011) Catabolic and anabolic actions of parathyroid hormone on the skeleton. *J. Endocrinol. Invest.* 34: 801–810.
15. Moen M D and Scott L J (2006) Recombinant full-length parathyroid hormone (1–84). *Drugs* 66: 2371–2381; discussion 2382–2375.
16. Cosman F, Nieves J W, and Dempster D W (2017) Treatment sequence matters: anabolic and antiresorptive therapy for osteoporosis. *J. Bone Miner. Res.* 32: 198–202.
17. Nakano T, Shiraki M, Sugimoto T, Kishimoto H, Ito M, Fukunaga M, Hagino H, Sone T, Kuroda T, and Nakamura T (2014) Once-weekly teriparatide reduces the risk of vertebral fracture in patients with various fracture risks: subgroup analysis of the Teriparatide Once-Weekly Efficacy Research (TOWER) trial. *J. Bone Miner. Metab.* 32: 441–446.
18. Sugimoto T, Shiraki M, Fukunaga M, Kishimoto H, Hagino H, Sone T, Nakano T, Ito M, Yoshikawa H, Minamida T, Tsuruya Y, and Nakamura T (2019) Study of twice-weekly injections of Teriparatide by comparing efficacy with once-weekly injections in osteoporosis patients: the TWICE study. *Osteoporos Int.* 30: 2321–2331.
19. Takakura A, Lee J W, Hirano K, Isogai Y, Ishizuya T, Takao-Kawabata R, and Iimura T (2017) Administration frequency as well as dosage of PTH are associated with development of cortical porosity in ovariectomized rats. *Bone Res.* 5: 17002.
20. Yamane H, Takakura A, Shimadzu Y, Kodama T, Lee J W, Isogai Y, Ishizuya T, Takao-Kawabata R, and Iimura T (2017) Acute development of cortical porosity and endosteal naive bone formation from the daily but not weekly short-term administration of PTH in rabbit. *PLoS ONE* 12: e0175329.
21. Parfitt A M, Drezner M K, Glorieux F H, Kanis J A, Malluche H, Meunier P J, Ott S M, and Recker R R (1987) Bone histomorphometry: standardization of nomenclature, symbols, and units. Report of the ASBMR histomorphometry nomenclature committee. *J. Bone Miner. Res.* 2: 595–610.
22. Dempster D W, Compston J E, Drezner M K, Glorieux F H, Kanis J A, Malluche H, Meunier P J, Ott S M, Recker R R, and Parfitt A M (2013) Standardized nomenclature, symbols, and units for bone histomorphometry: a 2012 update of the report of the ASBMR histomorphometry nomenclature committee. *J. Bone Miner. Res.* 28: 2–17.
23. Odin C, Guilbert T, Alkilani A, Boryskina O P, Fleury V, and Le Grand Y (2008) Collagen and myosin characterization by orientation field second harmonic microscopy. *Opt. Express* 16: 16151–16165.
24. Wu J P, Swift B J, Becker T, Squelch A, Wang A, Zheng Y C, Zhao X, Xu J, Xue W, Zheng M, Lloyd D, and Kirk T B (2017) High-resolution study of the 3D collagen fibrillary matrix of Achilles tendons without tissue labelling and dehydrating. *J. Microsc.* 266: 273–287.
25. Pijanka J K, Markov P P, Midgett D, Paterson N G, White N, Blain E J, Nguyen T D, Quigley H A, and Boote C (2019) Quantification of collagen fiber structure using second harmonic generation imaging and two-dimensional discrete Fourier transform analysis: application to the human optic nerve head. *J. Biophotonics* 12: e201800376.
26. Cicchi R, Vogler N, Kapsokalyvas D, Dietzek B, Popp J, and Pavone F S (2013) From molecular structure to tissue architecture: collagen organization probed by SHG microscopy. *J. Biophotonics* 6: 129–142.

27. Kiyomatsu H, Oshima Y, Saitou T, Miyazaki T, Hikita A, Miura H, Iimura T, and Imamura T (2015) Quantitative SHG imaging in osteoarthritis model mice, implying a diagnostic application. *Biomed. Opt. Express* 6: 405–420.
28. Saito M, Marumo K, Kida Y, Ushiku C, Kato S, Takao-Kawabata R, and Kuroda T (2011) Changes in the contents of enzymatic immature, mature, and non-enzymatic senescent cross-links of collagen after once-weekly treatment with human parathyroid hormone (1–34) for 18 months contribute to improvement of bone strength in ovariectomized monkeys. *Osteoporos Int.* 22: 2373–2383.
29. Yoshitake S, Mashiba T, Saito M, Fujihara R, Iwata K, Takao-Kawabata R, and Yamamoto T (2019) Once-weekly teriparatide treatment prevents microdamage accumulation in the lumbar vertebral trabecular bone of ovariectomized cynomolgus monkeys. *Calcif. Tissue Int.* 104: 402–410.
30. Glinkowski W M and Narloch J (2017) CT-scout based, semi-automated vertebral morphometry after digital image enhancement. *Eur. J. Radiol.* 94: 195–200.
31. Chou S H and Vokes T (2016) Vertebral morphometry. *J. Clin. Densitom.* 19: 48–53.
32. Wang X, Zauel R R, Rao D S, and Fyhrie D P (2008) Cancellous bone lamellae strongly affect microcrack propagation and apparent mechanical properties: separation of patients with osteoporotic fracture from normal controls using a 2D nonlinear finite element method (biomechanical stereology). *Bone* 42: 1184–1192.
33. Marotti G (1993) A new theory of bone lamellation. *Calcif. Tissue Int.* 53: S47–55; discussion S56.
34. Marotti G, Ferretti M, and Palumbo C (2013) The problem of bone lamellation: an attempt to explain different proposed models. *J. Morphol.* 274: 543–550.
35. Willett T L, Dapaah D Y, Uppuganti S, Granke M, and Nyman J S (2019) Bone collagen network integrity and transverse fracture toughness of human cortical bone. *Bone* 120: 187–193.
36. Depalle B, Qin Z, Shefelbine S J, and Buehler M J (2015) Influence of cross-link structure, density and mechanical properties in the mesoscale deformation mechanisms of collagen fibrils. *J. Mech. Behav. Biomed. Mater.* 52: 1–13.
37. Hamed E and Jasiuk I (2013) Multiscale damage and strength of lamellar bone modeled by cohesive finite elements. *J. Mech. Behav. Biomed. Mater.* 28: 94–110.
38. Hamed E, Jasiuk I, Yoo A, Lee Y, and Liszka T (2012) Multi-scale modelling of elastic moduli of trabecular bone. *J. R. Soc. Interface* 9: 1654–1673.
39. Sabet F A, Raeisi Najafi A, Hamed E, and Jasiuk I (2016) Modelling of bone fracture and strength at different length scales: a review. *Interface Focus* 6: 20150055.
40. Buehler M J (2008) Nanomechanics of collagen fibrils under varying cross-link densities: atomistic and continuum studies. *J. Mech. Behav. Biomed. Mater.* 1: 59–67.

Supplementary Figure1

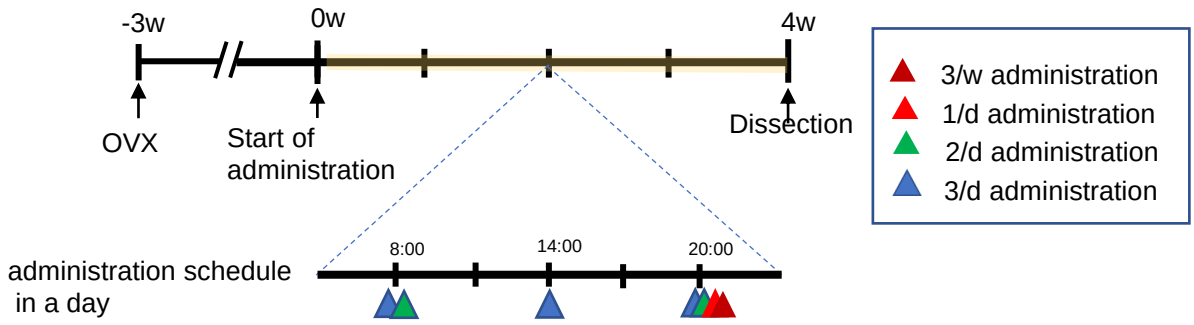

	Group	Operation	Treatment	Dose		Frequency	n
				(μg/kg)	(μg/kg/week)		
1	Sham	Sham	Vehicle	—	—	3/week	5
2	W3V	OVX	Vehicle	—	—	3/week	5
3	W3M	OVX	TPTD	6	18	3/week	5
4	W3H	OVX	TPTD	30	90	3/week	5
5	D1V	OVX	Vehicle	—	—	1/day	5
6	D1L	OVX	TPTD	1.2	8.4	1/day	5
7	D1M	OVX	TPTD	6	42	1/day	5
8	D1H	OVX	TPTD	30	210	1/day	5
9	D2V	OVX	Vehicle	—	—	2/day	5
10	D2L	OVX	TPTD	1.2	16.8	2/day	5
11	D2M	OVX	TPTD	6	84	2/day	5
12	D2H	OVX	TPTD	30	420	2/day	5
13	D3V	OVX	Vehicle	—	—	3/day	5
14	D3L	OVX	TPTD	1.2	25.2	3/day	5
15	D3M	OVX	TPTD	6	126	3/day	5

Supplementary Figure 2

(a)

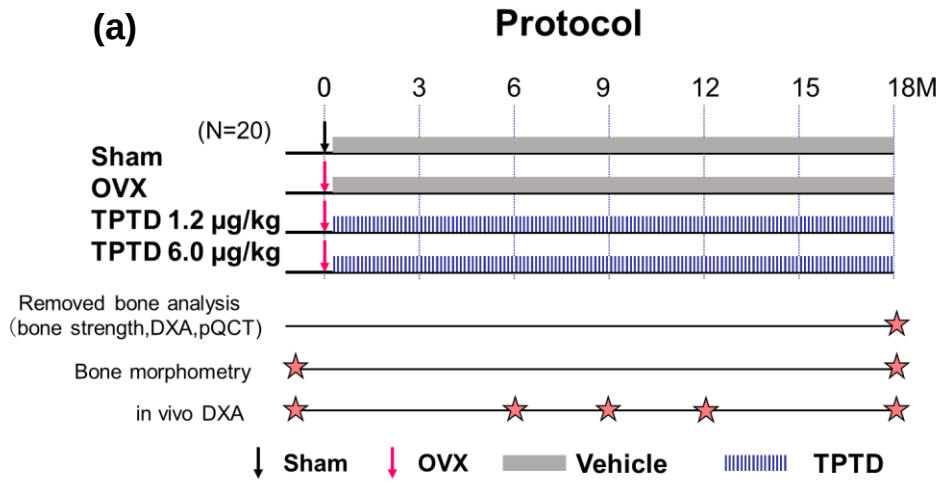

(b)

Group		Operation	Treatment	Dose	n
I	Sham	Sham	Vehicle	0 μg/kg	3
II	OVX	OVX	Vehicle	0 μg/kg	3
III	TPTD-L	OVX	TPTD	1.2 μg/kg	3
IV	TPTD-H	OVX	TPTD	6.0 μg/kg	3

(c)

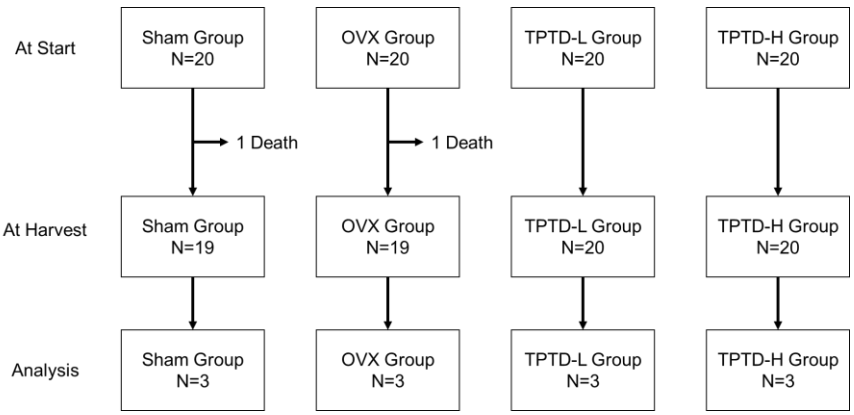

Supplementary Figure 3

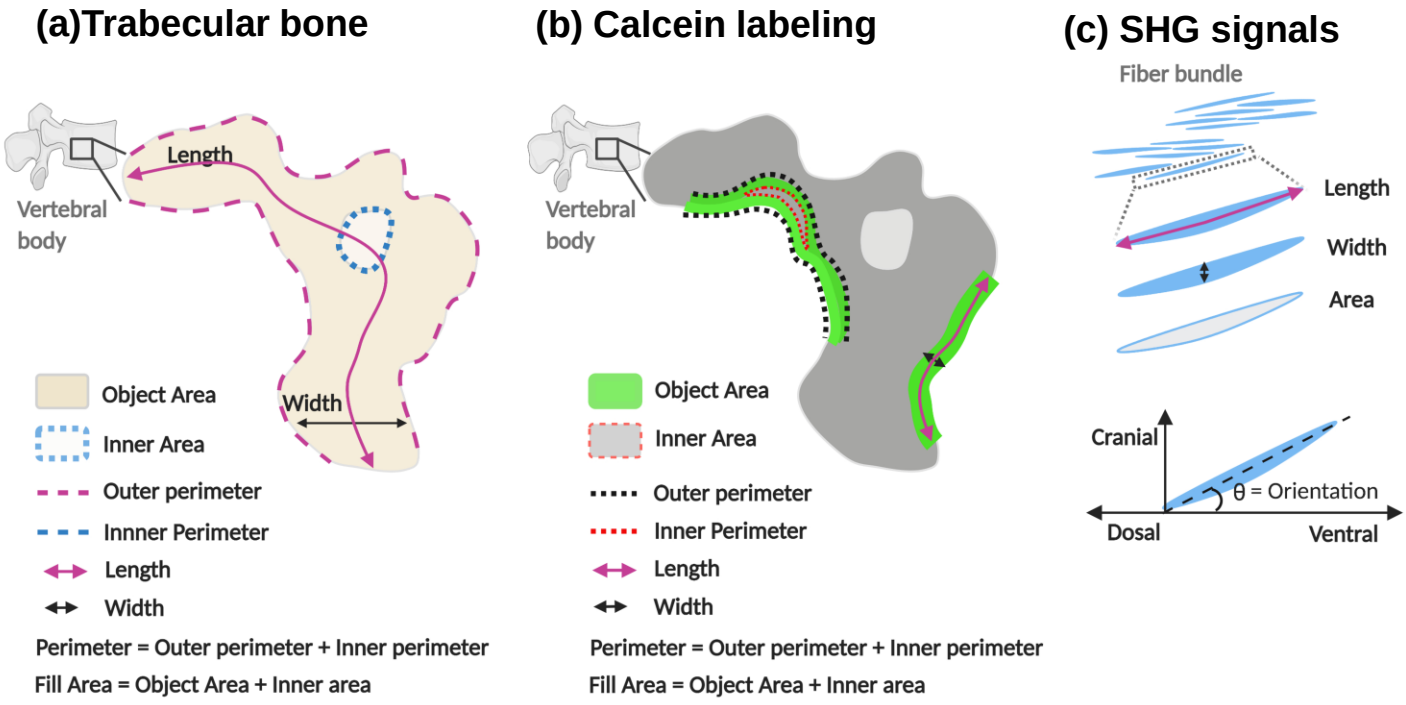

Supplementary Figure 4

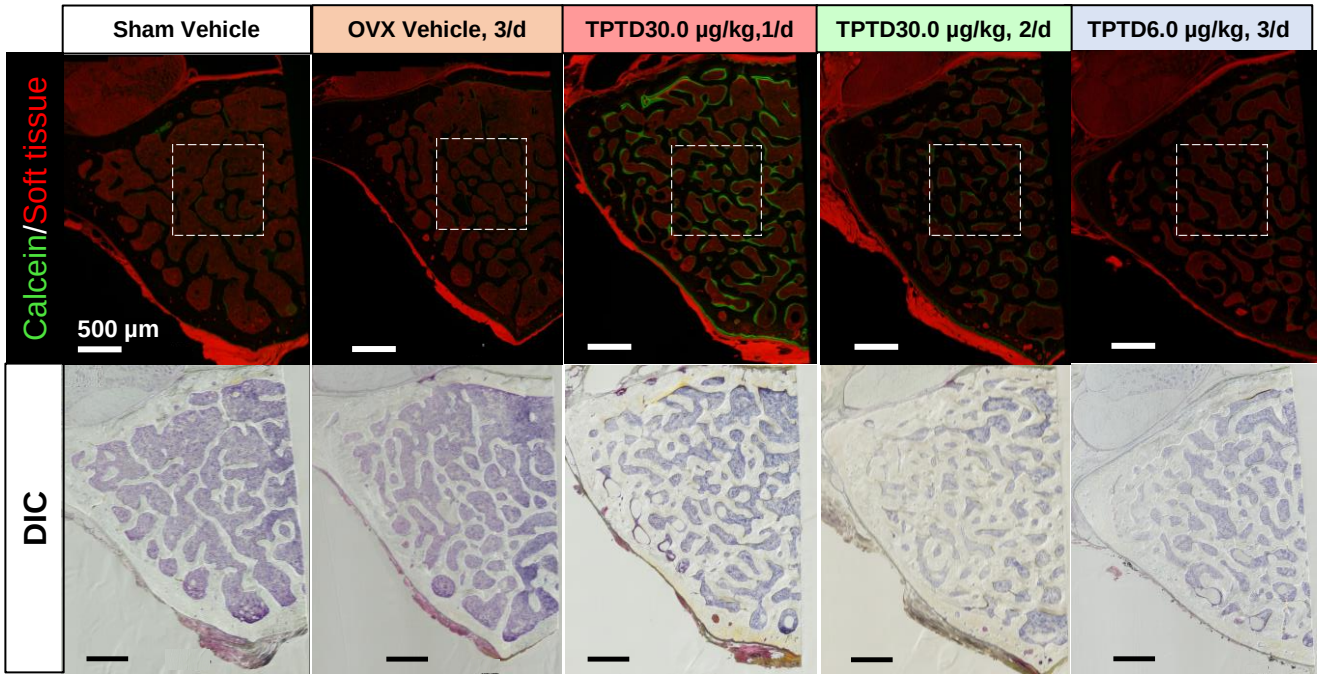

Supplementary Figure 5

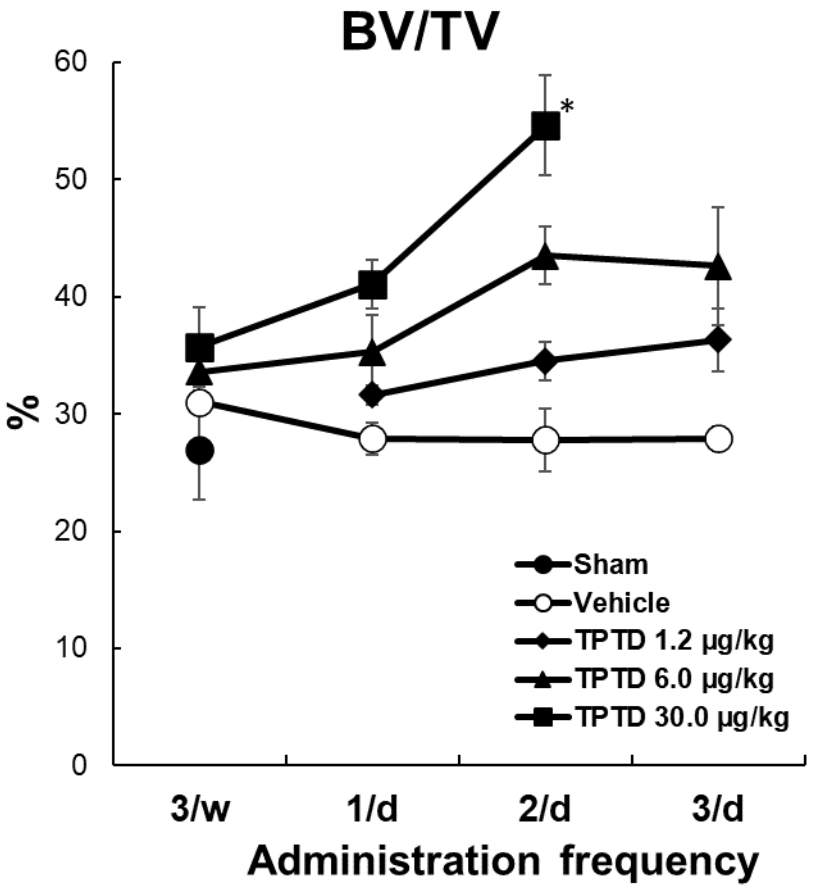

Supplementary Figure 6

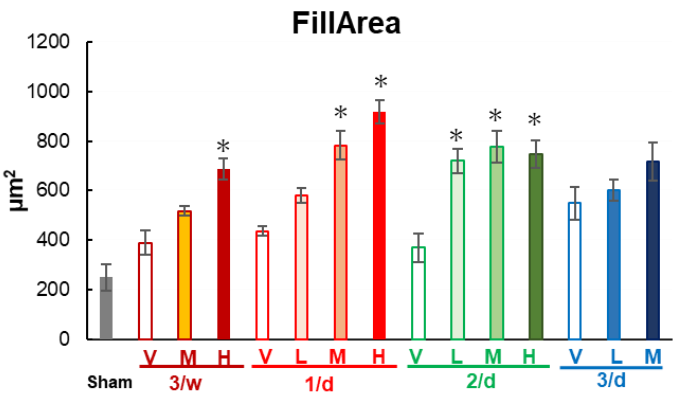

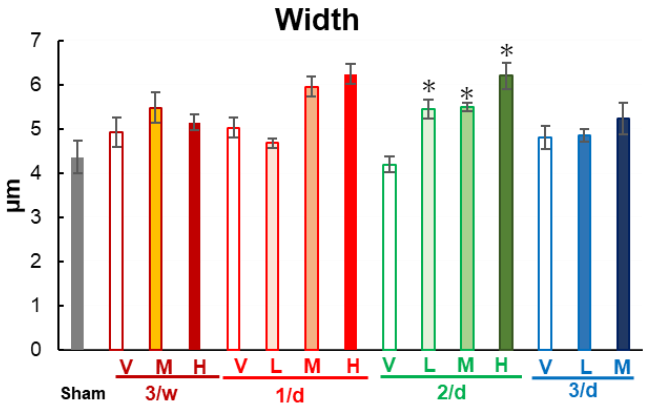

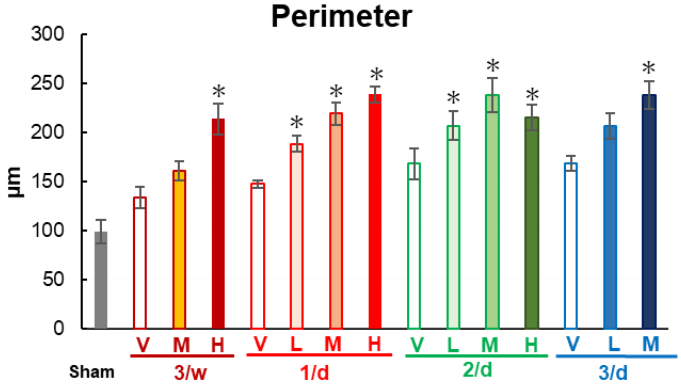

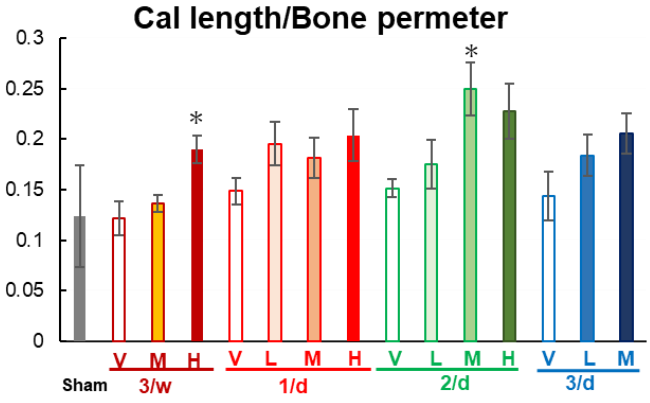

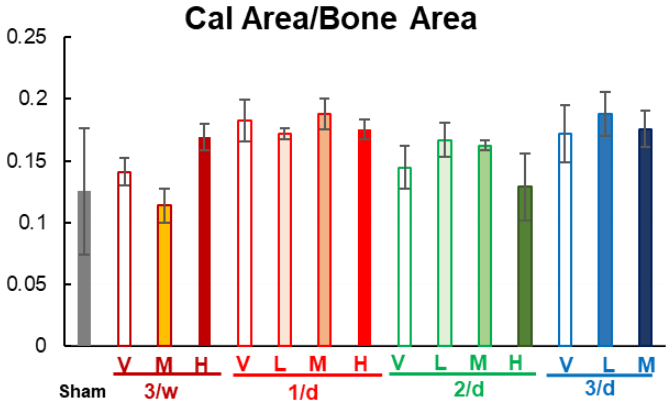

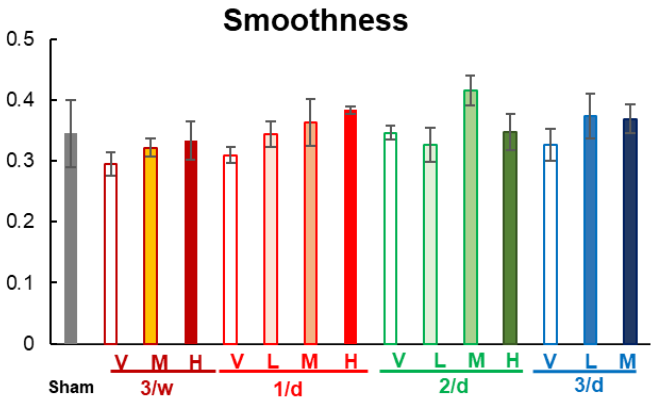

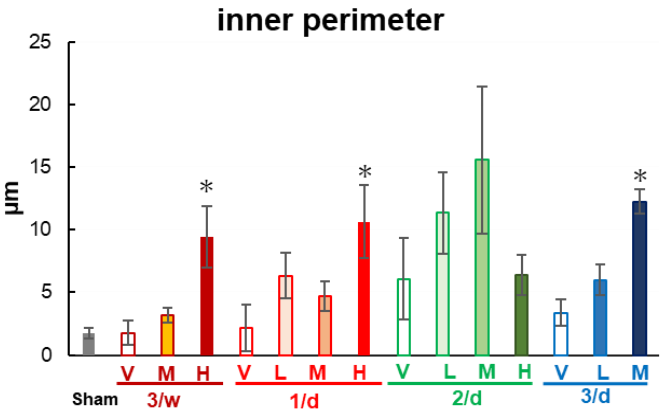

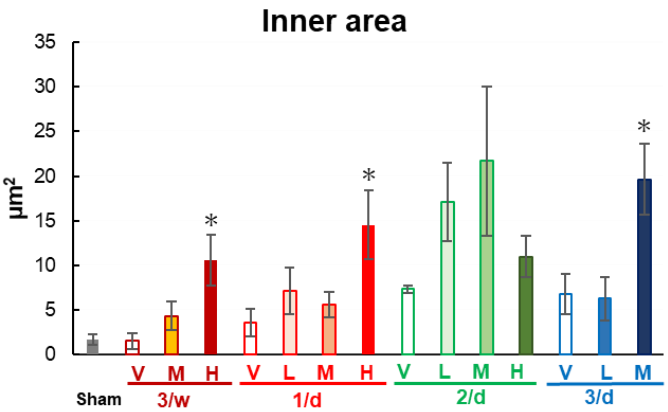

Supplementary Figure 7

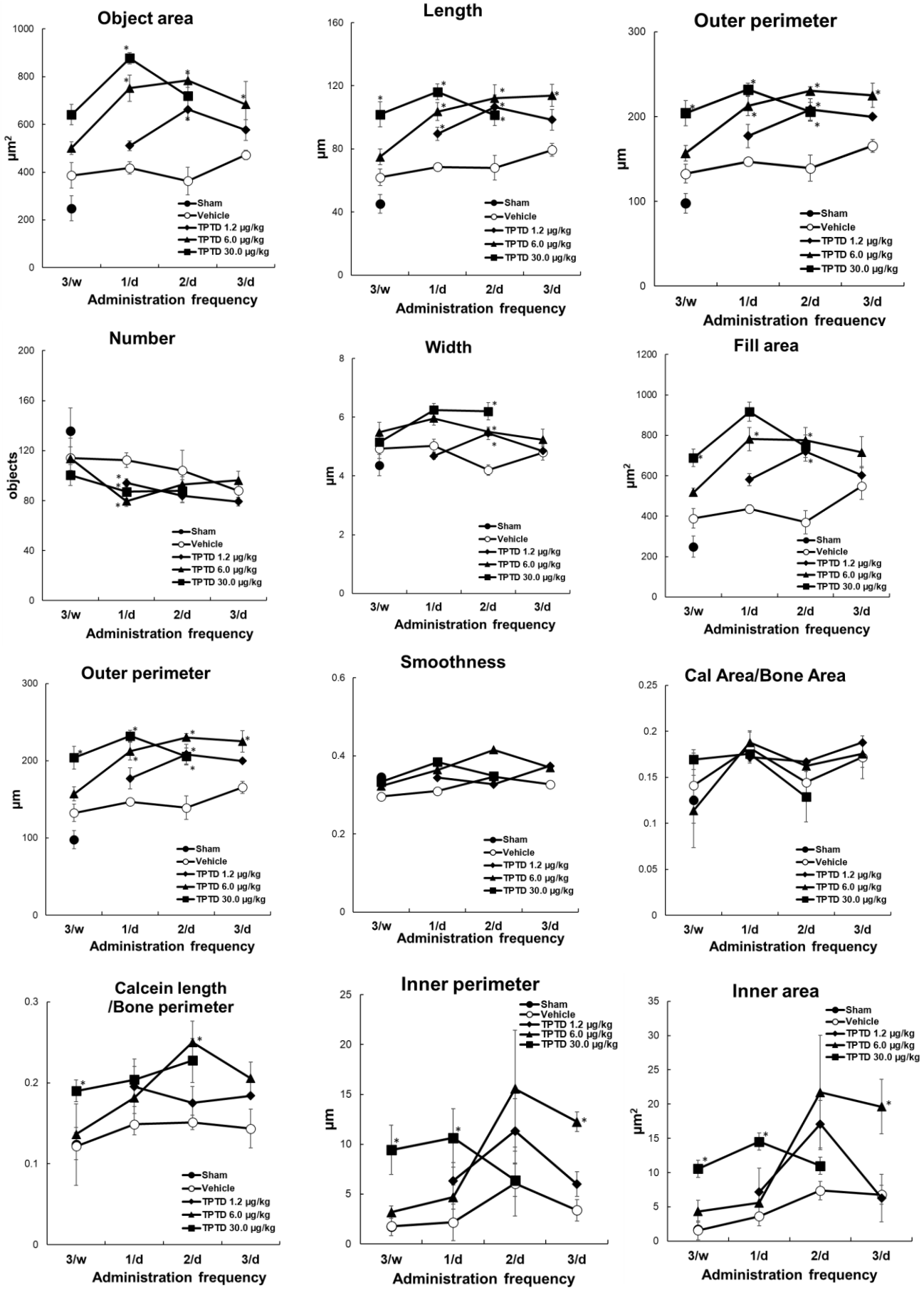

Supplementary Figure 8

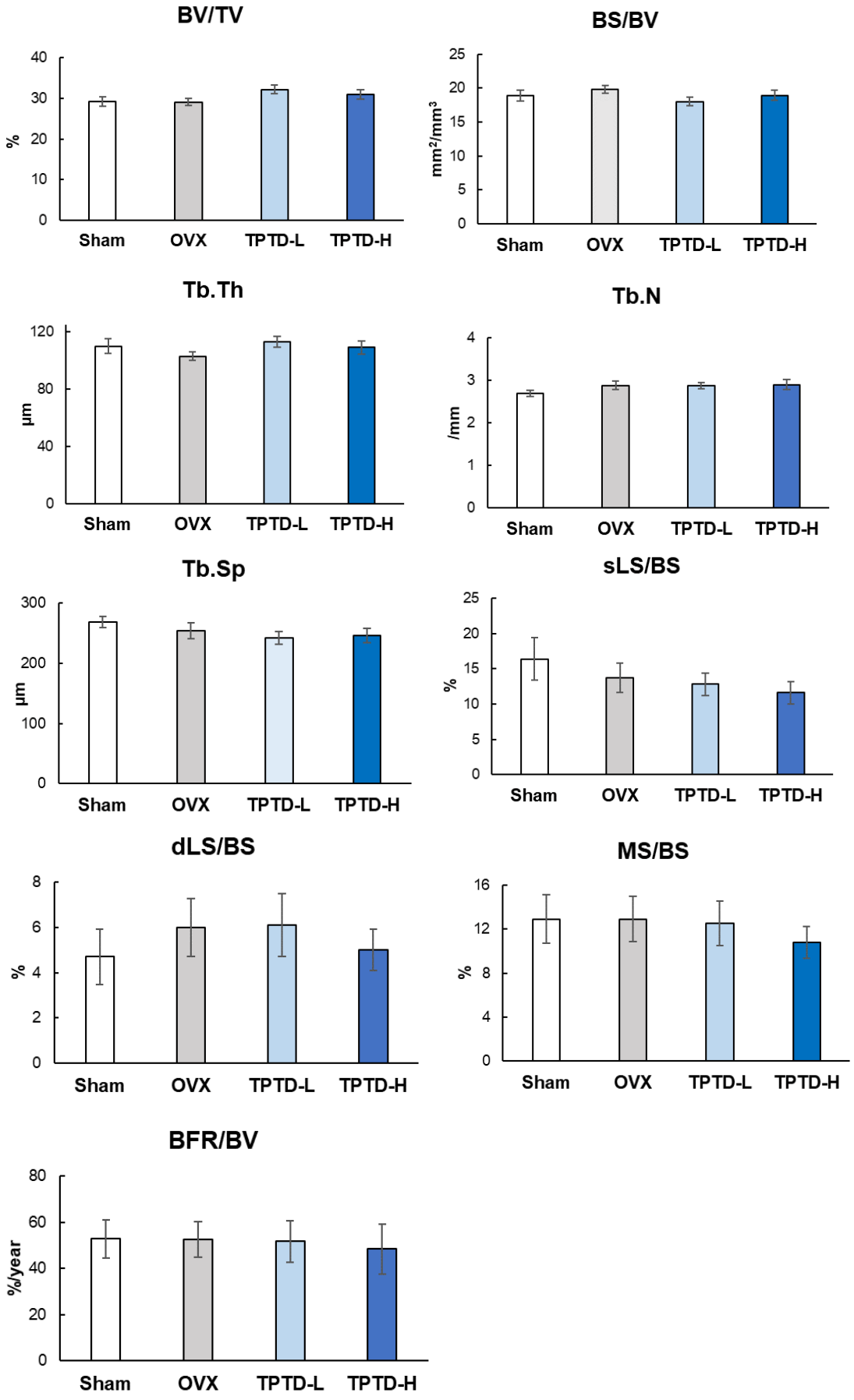

Supplementary Figure 9

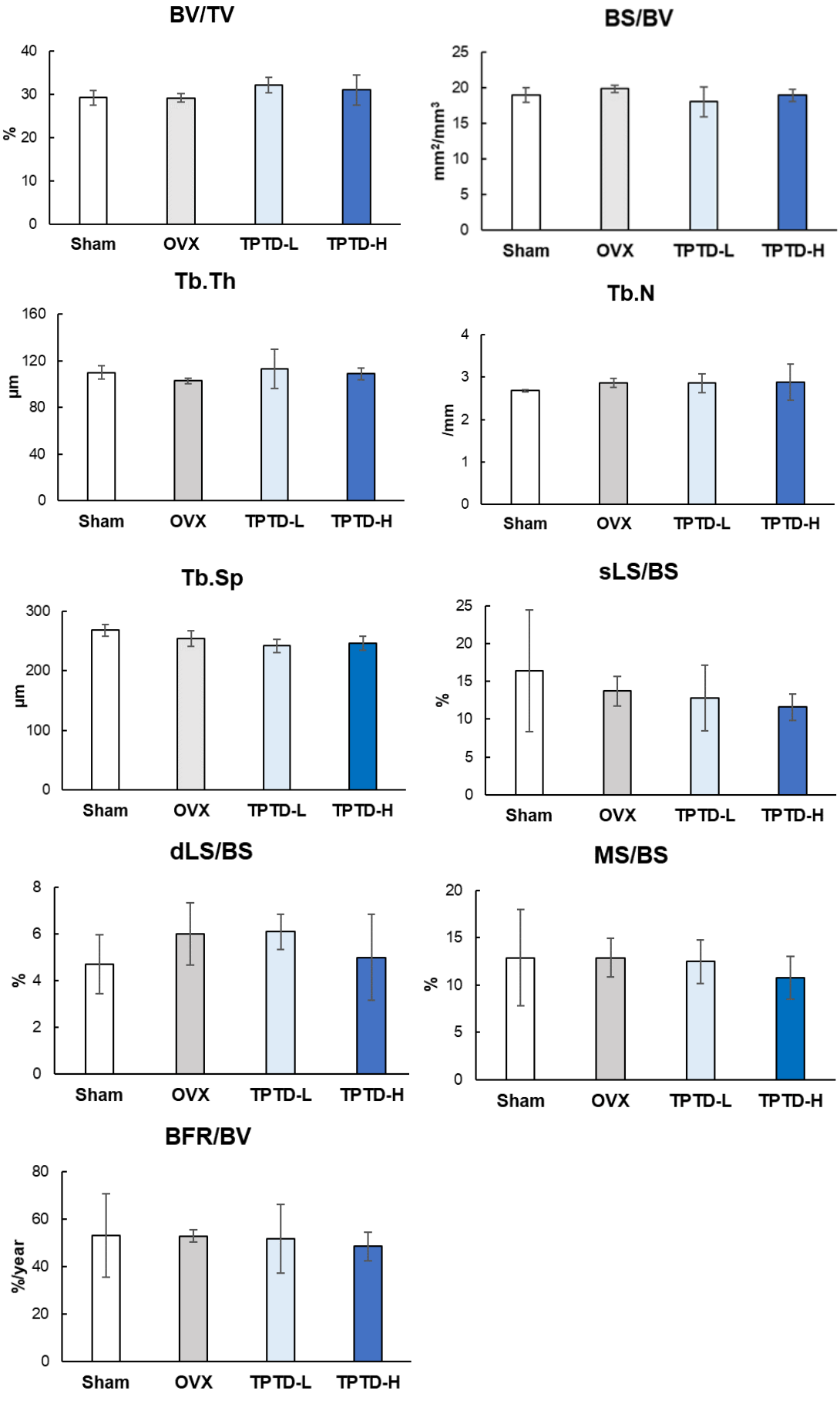

Supplementary Figure 10

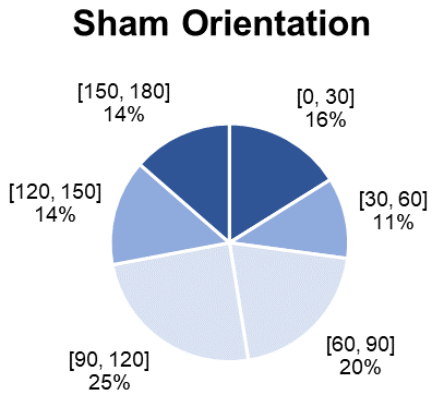

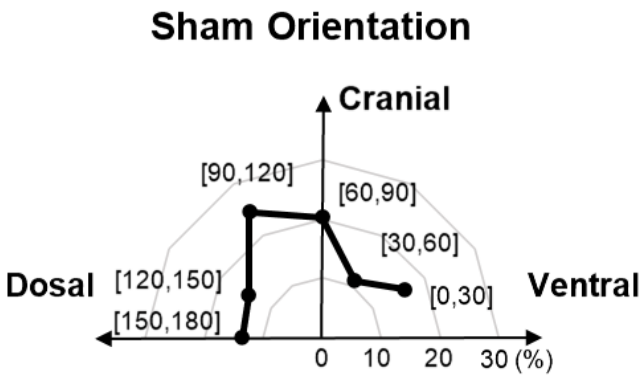

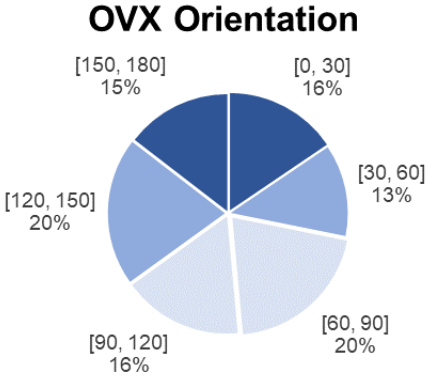

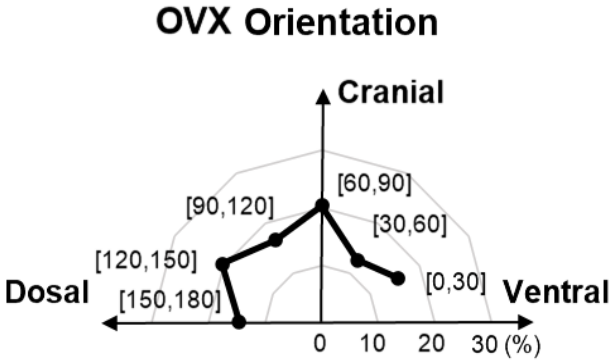

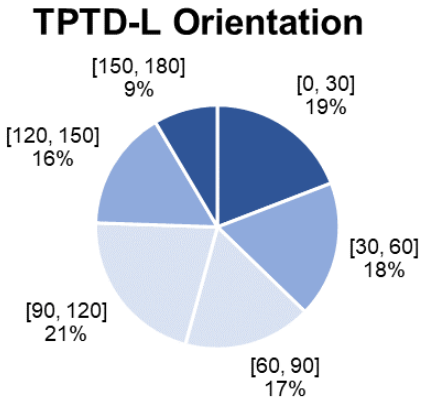

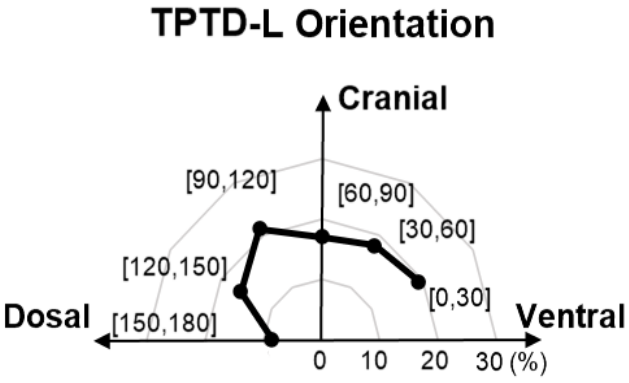

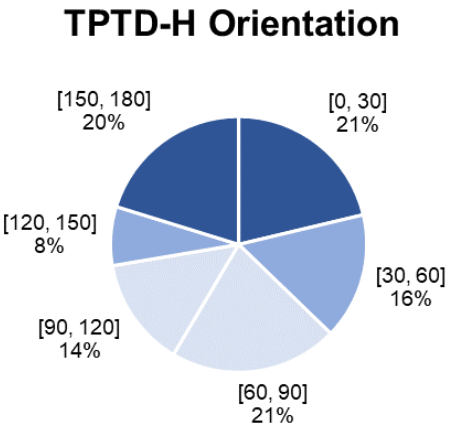

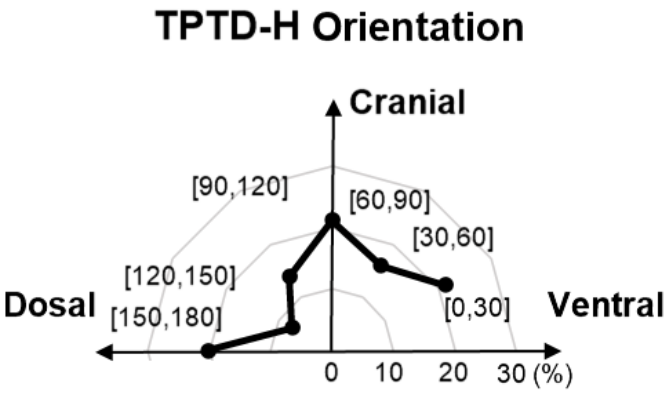

Supplementary Table 1

(a)

Parameter	units	Sham	OVX		
		Vehicle	Vehicle	TPTD	
				1.2 (μg/kg)	6.0 (μg/kg)
		(19)	(19)	(20)	(20)
BV/TV	(%)	29.2 ± 5.3	29.1 ± 3.8	32.2 ± 4.9	31.0 ± 5.1
BS/BV	(mm^2/mm^3)	18.9 ± 3.6	19.8 ± 2.6	18.0 ± 2.7	18.9 ± 3.3
Tb.Th	(μm)	110 ± 23	103 ± 13	113 ± 17	109 ± 20
Tb.N	(/mm)	2.68 ± 0.30	2.87 ± 0.43	2.86 ± 0.33	2.89 ± 0.51
Tb.Sp	(μm)	268 ± 42	254 ± 57	242 ± 48	246 ± 52
sLS/BS	(%)	16.4 ± 13.0	13.7 ± 9.0	12.8 ± 7.1	11.6 ± 7.0
dLS/BS	(%)	4.7 ± 5.3	6.0 ± 5.6	6.1 ± 6.2	5.0 ± 4.1
MS/BS	(%)	12.9 ± 9.6	12.9 ± 8.9	12.5 ± 9.1	10.8 ± 6.5
BFR/BV	(%/year)	52.8 ± 35.7	52.7 ± 33.7	51.7 ± 40.3	48.4 ± 49.1

(b)

Parameter	units	Sham	OVX		
		Vehicle	Vehicle	TPTD	
				1.2 (μg/kg)	6.0 (μg/kg)
		(3)	(3)	(3)	(3)
BV/TV	(%)	26.5 ± 2.9	28.1 ± 1.7	32.6 ± 3.1	33.1 ± 6.0
BS/BV	(mm^2/mm^3)	19.2 ± 1.8	19.8 ± 0.9	17.0 ± 3.6	18.4 ± 1.5
Tb.Th	(μm)	105 ± 10	101 ± 4	121 ± 29	109 ± 9
Tb.N	(/mm)	2.53 ± 0.05	2.78 ± 0.18	2.74 ± 0.38	3.07 ± 0.74
Tb.Sp	(μm)	291 ± 16	260 ± 23	248 ± 26	228 ± 65
sLS/BS	(%)	20.4 ± 13.9	11.1 ± 3.4	13.0 ± 7.6	8.5 ± 3.0
dLS/BS	(%)	4.9 ± 2.2	3.9 ± 2.3	2.7 ± 1.3	4.8 ± 3.2
MS/BS	(%)	15.1 ± 8.8	9.5 ± 3.5	9.2 ± 4.0	9.1 ± 3.9
BFR/BV	(%/year)	56.5 ± 30.5	37.8 ± 4.5	43.3 ± 25.1	34.0 ± 10.4

Supplementary Figure Legends

Fig. S1 The time course and regimen settings of TPTD administration and sampling in ovariectomized rats. Rats at 13 weeks of age were subjected to either ovariectomy or sham surgery. At three weeks after the surgery, the administration of TPTD was started and continued for 4 weeks.

Fig. S2 The time course and regimen settings of TPTD administration and sampling in ovariectomized monkeys. (a) Monkeys (age:12.0 ±1.5 years, weight:2.06-3.48 kg) were subjected to either ovariectomy or sham surgery. At one week after surgery, the administration of TPTD was started. TPTD at the indicated doses or saline as a vehicle was subcutaneously injected once a week, for 18 months. (b) Monkeys were divided into four groups (n=19 to 20): (1) Sham group, (2) OVX group, (3) TPTD-L group; OVX with low-dose teriparatide (1.2 μg/kg), and (4) PTH-H group; OVX with high-dose teriparatide (6.0 μg/kg). (c) Three specimens from each of the 4 regimen groups (19 to 20 specimens) that showed histomorphometric scores nearest to the mean value were selected for SHG imaging and a further semi-automatic imaging analysis.

Fig. S3 The parameter settings for semi-quantitative fluorescence morphometry. The

topological parameters for (a) trabecular bone, (b) calcein-labelling, and (c) collagen fibers were established with the application of commercially available image analysis tools (NIS-Elements AR and NIS.ai, Nikon, Tokyo, Japan).

Fig. S4 Representative large tiling fluorescence images and corresponding DIC images of horizontal bone sections of rat vertebral bodies.Representative DIC (left panels) and corresponding fluorescence images of rat vertebral trabeculae treated with the indicated TPTD regimens. (Upper panels) Representative large tiling fluorescence images (calcein and autofluorescence, in green and red, respectively) of rat vertebral trabeculae treated with the indicated TPTD regimens. (Lower panels) Corresponding DIC images. White-dotted squares demonstrate the positions of the ROI shown in Figure 2. Scale bars indicate 500 μm.

Fig. S5 The anabolic effect of TPTD on the bone volume of rat vertebral trabeculae. Quantitative and statistical analyses of bone volume / tissue volume (BV/TV) by a semi-automatic recognition system. The average of BV/TV plotted against the administration frequency. Data are shown as the mean ± S.E.

* Indicates $p<0.05$ vs. vehicle for each the frequency of administration (Dunnett's test).

Fig. S6 The quantitative topological analysis of bone formation pattern by morphometry of calcein signals in rat vertebral trabeculae. The average of indicated parameters were statistically compared according to the frequency of administration. Data are shown as the mean ± S.E. * Indicates $p<0.05$ vs. vehicle for each the frequency of administration (Dunnett's test).

Fig. S7 The quantitative topological analysis of bone formation patterns by morphometry of calcein signals in rat vertebral trabeculae. The average values of the indicated parameters were plotted against the frequency of administration. Data are shown as the mean ± S.E. * Indicates $p<0.05$ vs. vehicle for each the frequency of administration (Dunnett's test).

Fig. S8 Bone histomorphometry of monkey vertebral trabeculae (analyses of whole specimens). The indicated histomorphometric parameters were scored and compared across 4 experimental groups using whole samples. Data are shown as the mean ± S.E. P-values vs. OVX group (Dunnett's test) did not show statistical significance ($p>0.05$).

Fig. S9 Bone histomorphometry of monkey vertebral trabeculae (analyses of 3 specimens selected from the TPTD regimen groups). The indicated histomorphometric parameters were scored and compared across 4 experimental groups using 3 samples selected from each group. Data are shown as the mean ± S.E. P-values vs. OVX group (Dunnett's test) did not show statistical significance ($p>0.05$).

Fig. S10 The orientation analyses of bone collagen in monkey vertebral trabeculae. The orientation analysis of SHG signal derived fibrous collagen was conducted and comparisons were made across 4 groups (see Supplementary Figure 3 c). Pie charts demonstrate the horizontal and vertical directions in dark and light blue, respectively (right panels). Notably, this parameter analysis indicates the anisotropy of collagen-derived signals, especially in the OVX groups.

Table S1 Bone histomorphometry of monkey vertebral trabeculae. (a) analyses of whole specimens (b) analyses of 3 specimens selected from the TPTD regimen groups.

謝辞

本研究の構想、データ解析、論文執筆に至るまで、北海道大学大学院歯学研究院薬理学教室飯村忠浩教授には終始一貫して適切な助言と丁寧なご指導をしていただきました。甚大なる感謝の意を表します。
本研究の論文執筆にあたり、同研究室の李智媛助教には、細部に渡るご指導ならびにたくさんの有益な助言をいただきました。深く感謝の意を表します。
本研究の実験、データ解析ならびに考察につきまして、旭化成ファーマ株式会社高尾亮子博士ならびに高倉綾博士には、骨組織解析および PTH 製剤の先進的な知見をご教授していただきました。深く感謝の意を表します。
本研究のデータ解析につきまして、株式会社ニコン徳永和明博士ならびに松森はるか博士には、先進的な画像解析手法をご教授していただきました。深く感謝の意を表します。
また、ここに記しきれない多くの方々の学恩、ご支援によって本研究が成立していることを銘記し、心より感謝の意を表します。